HHS Public Access

Author manuscript

J Physiol. Author manuscript; available in PMC 2024 August 01.

Published in final edited form as:

J Physiol. 2023 August ; 601(16): 3667–3686. doi:10.1113/JP284960.

The astrocytic Na^+-HCO_3^- cotransporter, NBCe1, is dispensable for respiratory chemosensitivity

Keyong Li,

Elizabeth C. Gonye,

Ruth L. Stornetta,

Christopher B. Bayliss,

Grace Yi,

Daniel S. Stornetta,

Serapio M. Baca,

Stephen B.G. Abbott,

Patrice G. Guyenet,

Douglas A. Bayliss*

Department of Pharmacology, University of Virginia, Charlottesville, VA, USA, 22908

Abstract

The interoceptive homeostatic mechanism that controls breathing, blood gases and acid-base balance in response to changes in CO_2/H^+ is exquisitely sensitive, with convergent roles proposed for chemosensory brainstem neurons in the retrotrapezoid nucleus (RTN) and their supporting glial cells. For astrocytes, a central role for NBCe1, a Na^+-HCO_3^- cotransporter encoded by *Slc4a4*, has been envisaged in multiple mechanistic models (i.e., underlying enhanced CO_2-induced local extracellular acidification or purinergic signaling). We tested these NBCe1-centric models by using conditional knockout mice in which *Slc4a4* was deleted from astrocytes. In GFAP-Cre;*Slc4a4*$^{fl/fl}$ mice we found diminished expression of *Slc4a4* in RTN astrocytes by comparison to control littermates, and a concomitant reduction in NBCe1-mediated current. Despite disrupted NBCe1 function in RTN-adjacent astrocytes from these conditional knockout mice, CO_2-induced activation of RTN neurons or astrocytes *in vitro* and *in vivo*, and CO_2-stimulated breathing was indistinguishable from NBCe1-intact littermates; hypoxia-stimulated breathing and sighs were likewise unaffected. We obtained a more widespread deletion of NBCe1 in brainstem astrocytes by using tamoxifen-treated Aldh1l1-Cre/ERT2;*Slc4a4*$^{fl/fl}$ mice. Again, there was no difference in effects of CO_2 or hypoxia on breathing or on neuron/astrocyte activation in NBCe1-deleted mice. These data indicate that astrocytic NBCe1 is not required for the respiratory responses to these chemoreceptor stimuli in mice, and that any physiologically relevant astrocytic contributions must involve NBCe1-independent mechanisms.

*correspondence to dab3y@virginia.edu.

Author Contributions

KYL, RLS, PGG, and DAB designed research; KYL, RLS, CBB, DSS, SMB performed research; KYL, ECG, RLS, CBB, GY, SMB, and DAB analyzed data; and all authors edited and approved the final version of the manuscript.

Authors competing interest statement

All authors declare no competing interests.

Graphical Abstract

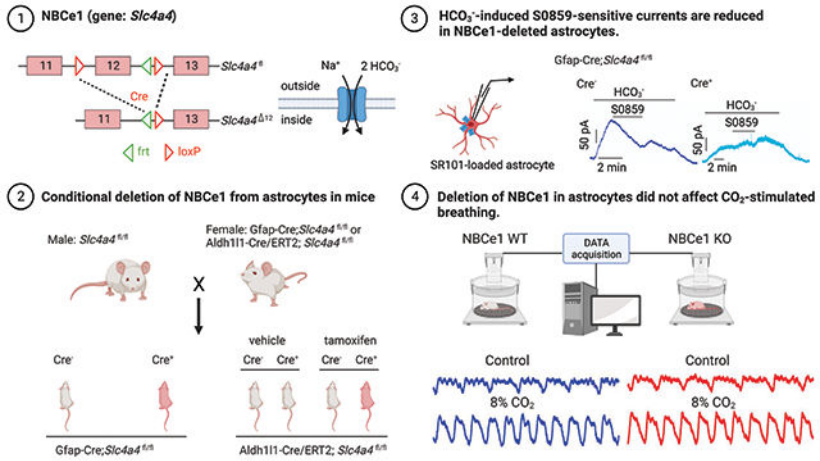

Astrocytic NBCe1 expression is not required for CO_2-stimuated breathing in mice.

Mice bearing “floxed” alleles for *Slc4a4*, the gene that encodes the NBCe1 electrogenic Na^+-HCO_3^- co-transporter, were crossed with two different lines of mice that express Cre recombinase preferentially in astrocytes. After conditional knockout of *Slc4a4*, NBCe1-like currents were eliminated from astrocytes, but CO_2-stimulated breathing was unaffected. Thus, contrary to a prominent current hypothesis, astrocytic NBCe1 does not appear to play a role in CO_2-stimulated breathing, and alternative mechanisms should be sought to explain proposed astrocytic contributions to this respiratory chemoreflex.

Keywords

retrotrapezoid; astrocyte; *Slc4a4* ; electrogenic; depolarization-induced alkalosis; chemosensors

Introduction

The RTN neurons in the ventral parafacial region of the rodent brainstem contribute to direct sensing of CO_2/H^+ in service of homeostatic regulation of breathing, representing an anatomic substrate for the long-sought ventral medullary central chemoreceptors (Mulkey et al., 2004; Guyenet & Bayliss, 2015; Guyenet et al., 2019). The central respiratory chemoreflex – increased breathing in response to elevated CO_2 – is exquisitely sensitive, and multiple mechanisms have been proposed to account for this sensitivity (Guyenet & Bayliss, 2015; Guyenet et al., 2019). These include direct actions of intrinsically chemosensory RTN neurons, as well as indirect modulatory actions by other chemosensory neurons and glia that are largely intermediated by RTN neurons (Gourine et al., 2010; Hodges & Richerson, 2010; Guyenet & Bayliss, 2015; Hawkins et al., 2017; Souza et al., 2018; Guyenet et al., 2019). Irrespective of whether their excitation arises from direct or indirect CO_2/H^+ sensing mechanisms, chemosensitive RTN neurons convey a facilitatory drive onward to the various respiratory centers that dictate the rate and depth of breathing (Guyenet & Bayliss, 2015; Del Negro et al., 2018; Guyenet et al., 2019).

For RTN neurons, the intrinsic pH sensing mechanism has been attributed to two molecular proton detectors – TASK-2 and GPR4 – that together contribute a major component of the overall chemosensitivity (Gestreau et al., 2010; Wang et al., 2013; Guyenet & Bayliss, 2015; Kumar et al., 2015; Guyenet et al., 2019). For the proposed glial contributions, the molecular mechanisms are less certain, but increased activity of an electrogenic Na^+-HCO_3^- co-transporter, NBCe1 (encoded by *Slc4a4*) has been proposed to play a critical role in two different non-exclusive processes initiated by RTN astrocytes: 1) "proton boosting" whereby local pH changes are amplified (Chesler, 2003; Erlichman et al., 2008; Guyenet & Bayliss, 2015; Guyenet et al., 2019); and 2) purinergic paracrine signaling, based on astrocytic ATP release (Gourine et al., 2010; Turovsky et al., 2016). A separate NBCe1-independent mechanism involving direct activation of astrocytic, ATP-releasing connexin hemichannels by CO_2 has also been suggested to contribute to local purinergic signaling (Huckstepp et al., 2010a; Huckstepp et al., 2010b; Meigh et al., 2013).

For the two proposed NBCe1-dependent astrocytic mechanisms, intracellular acidification and/or membrane depolarization induced by CO_2 increases NBCe1 activity, resulting in enhanced HCO_3^- transport into the astrocyte (Grichtchenko & Chesler, 1994; Chesler, 2003; Turovsky et al., 2016; Theparambil et al., 2017), effectively removing proton buffering equivalents from the extracellular space (Erlichman et al., 2008; Wenker et al., 2010; Mulkey & Wenker, 2011; Guyenet & Bayliss, 2015; Guyenet et al., 2019). Concurrently, the increased NBCe1 activity also promotes entry of Na^+ ions, driving a secondary Na-Ca exchange mechanism that provides the Ca^{2+} needed for ATP release (Turovsky et al., 2016). In the latter instance, ATP-mediated purinergic signaling either directly activates RTN neurons (Gourine et al., 2010), or it causes a local vasoconstriction to reduce washout of metabolic byproducts (i.e., CO_2), further enhancing acidification (Guyenet & Bayliss, 2015; Hawkins et al., 2017; Guyenet et al., 2019). Accordingly, because of its central position in these proposed mechanisms, deletion of NBCe1 from astrocytes is expected to eliminate its contributions to glial respiratory chemosensation and thereby reduce CO_2-stimulated breathing.

To test these proposed mechanisms, we used two different Cre driver lines to generate conditional deletion in mouse astrocytes of *Slc4a4*, the gene encoding NBCe1. Despite suppressing *Slc4a4* expression and NBCe1-associated currents in astrocytes, we found no effect of astrocytic *Slc4a4* depletion on CO_2-induced RTN neuronal activation or CO_2-stimulated ventilation; hypoxia-activated breathing and sighs were also unaffected. Based on these results, we conclude that NBCe1-mediated astrocytic mechanisms are not required for respiratory chemosensitivity in mice.

Material and Methods

Ethical Approval.

Experiments were performed following procedures adhering to National Institutes of Health Animal Care and Use Guidelines and approved by the Animal Care and Use Committee of the University of Virginia (Protocol #2454). The investigators understand the ethical principles under which the journal operates, and this work complies with the animal ethics checklist as outlined by the journal (Percie du Sert et al., 2020).

Animals.

Experiments were performed on mice of either sex. Mice were housed in HEPA-ventilated racks and steam-sterilized caging (up to 5 per cage), with *ad libitum* access to food and water. Animals were exposed to 12 h light/dark cycles in a vivarium maintained at 22-24°C and ~40-50% relative humidity. For electrophysiological recordings from RTN neurons and RTN-adjacent astrocytes, we used a Phox2b-GFP BAC transgenic mouse line (Jx99) in which GFP expression is driven by the Phox2b promoter; these mice were developed by the GENSAT project, maintained in-house, and characterized previously (Lazarenko et al., 2009). A conditional deletion-ready mouse line was obtained in which exon 12 of *Slc4a4*, the gene encoding NBCe1, was flanked by loxP sites (kindness of Dr. Gary E. Shull, University of Cincinnati); the "floxed" exon is included in all splice variants of NBCe1 (Vairamani et al., 2018). We knocked out NBCe1 in astrocytes by crossing, in-house, the "floxed" *Slc4a4* mice with either GFAP-Cre transgenic mice (RRID:IMSR_JAX:012886) (Garcia et al., 2004) or tamoxifen-inducible Aldh1l1-Cre/ERT2 BAC transgenic mice (RRID:IMSR_JAX:031008) (Winchenbach et al., 2016); after intercrossing Cre-positive offspring heterozygous at the *Slc4a4* locus, we established breedings between Cre-positive female $Slc4a4^{fl/fl}$ and Cre-negative male $Slc4a4^{fl/fl}$ mice to obtain homozygous male and female $Slc4a4^{fl/fl}$ littermates that were either Cre-negative or Cre-positive (GFAP line, N=male: Cre^{-}, 24; Cre^{+}, 30; N=female: Cre^{-}, 40; Cre^{+}, 36; Aldh1l1 line, N=male: Cre^{-}: 53, Cre^{+}, 39; N=female: Cre^{-}, 20; Cre^{+}, 35). To induce Cre expression in Aldh1l1-CreERT2 mice, adult mice (>70 days old) were treated for 10 consecutive days with tamoxifen (150 μl/mouse/day, ip, from 20 mg/ml stock in peanut oil; Sigma-Aldrich, St. Louis, MO); the vehicle and tamoxifen-treated mice were studied after 3 weeks. All studies were performed and analyzed by individuals blinded to genotype and experimental treatment.

Breathing measurements.

Ventilatory variables were measured in conscious adult mice by whole body plethysmography, following manufacturer instructions (EMKA Technologies, Sterling, VA) and as previously described (Kumar et al., 2015; Shi et al., 2016). A mass flow regulator provided quiet, constant and smooth flow through the animal chamber (0.5 L/min), and the pressure transducers were calibrated by injecting a known volume of air with a syringe into the chamber (10 ml, <2 s). Mice were habituated to plethysmography chambers maintained at 25-28°C for 4 h at least one day prior to testing. The protocol included three sequential incrementing CO_2 challenges (7 min exposures to 2%, 4%, 6%, 8% CO_2, combined with 60% O_2, balance N_2; each separated by 5 min of 60% O_2/40% N_2). Hypercapnic exposure was performed in hyperoxia to minimize contributions of peripheral chemoreceptors to the hypercapnic ventilatory reflex (Basting et al., 2015) and to attribute ventilatory effects to central chemoreceptors. For hypoxia challenges, mice were exposed to 10% O_2, balance N_2 for up to 5 min.

Analysis of ventilatory responses.

Ventilatory flow signals were recorded, amplified, digitized and analyzed using Iox 2.7 (EMKA Technologies) to determine ventilatory parameters over sequential 20s epochs (~50 breaths), during periods of behavioral quiescence and regular breathing. Minute ventilation

(V_E, ml/min) was calculated as the product of respiratory frequency (fR, breaths/min) and tidal volume (V_T, ml/breath), and normalized to body weight. In short, for each breath, Iox software determines inspiratory time (Ti) and expiratory time (Te) from the zero-flow crossing time point as the flow trace alternates between negative (inspiration) and positive (expiration) values, and breathing frequency is calculated from the sum of Ti and Te. The area under the flow curve during inspiration (i.e., below the zero-flow point) is taken as V_T. For analysis of the hypercapnic ventilatory response, we sampled 10 consecutive epochs (200s, representing ~400–500 breaths at rest) that showed the least inter-breath irregularity during the steady-state plateau period after each CO_2 exposure, as determined by Poincaré analysis (Loria et al., 2013; Kumar et al., 2015). The response to hypoxia (10% O_2) was determined from the peak V_E (20 s epoch) within the 5 min of exposure to the hypoxic gas mixture, and the incidence of hypoxia-induced sighs was determined throughout the last 3 min of hypoxic exposure (Kumar et al., 2015). There were no Cre- and/or tamoxifen-dependent differences in breath-to-breath variability measured at any level of CO_2 or O_2 in the different mouse lines (i.e., Poincaré ellipse method; Loria et al., 2013).

Fos expression after exposure to hypercapnia in vivo.

Activation of RTN neurons and astrocytes by elevated CO_2 or O_2 was assessed by *Fos* expression (Shi et al., 2016; Shi et al., 2017). In short, adult mice were habituated to the plethysmography chamber for 1 h in hyperoxia (60% O_2, balance N_2) before an additional 35 min exposure to hyperoxia (60% O_2, balance N_2) or hypercapnia (12% CO_2, 60% O_2, balance N_2). Immediately following exposure to the test condition, mice were anesthetized (ketamine, 75 mg/kg; xylazine, 5 mg/kg; IP), examined for absence of response to a firm toe pinch and perfused transcardially (as below). All experiments, including the histology, were run in pairs (i.e., mice exposed to hypercapnia and hyperoxia). Sections were prepared for multiplex fluorescence *in situ* hybridization, as described below.

Multiplex fluorescence in situ hybridization (FISH).

Mice were anesthetized with ketamine/xylazine (75 mg/kg, 5 mg/kg; IP), examined for absence of response to a firm toe pinch and perfused transcardially with 4% PFA/0.1 M PB. Brains and kidneys were removed, immersed in the same fixative for 16-18 hours at 4°C, cut in the transverse plane (30 μm) and placed in cryoprotectant (30% ethylene glycol, 20% glycerol, 50 mM sodium phosphate buffer, pH 7.4) at −20°C until further processing. Tissue preparation and staining procedure utilized the RNAscope® Multiplex Fluorescent Assay (Advanced Cell Diagnostics, Hayward, CA; RRID:SCR_012481), according to manufacturer instructions and as previously described (Shi et al., 2017). Catalog probes were used for *Aldh1l1*, *Nmb*, *Gfap*, *Slc4a5*, and *Fos*, whereas a custom *Slc4a4* probe was specifically designed to encompass the floxed exon 12 that was deleted by Cre-mediated excision (Cat. #533358). Following hybridization, sections were air-dried, counterstained with ProLong™ Gold antifade reagent containing DAPI, and coverslipped for further analysis.

Cell counts and analysis.

Serial coronal sections (1:3 series) through the rostrocaudal extent of the RTN were mounted on glass slides, and images were acquired using an epifluorescence microscope (Zeiss

Axioimager Z1) equipped with Neurolucida software (MBF Bioscience, Williston, VT). One section from each mouse was used for cell counts and was chosen from the rostrocaudal level where maximal numbers of RTN neurons are located (6.48 mm caudal to bregma; (Shi et al., 2017). In the two mouse lines, there were no Cre- and/or tamoxifen-dependent differences in the average number of RTN neurons counted from these sections (44.2 ± 12.7 Nmb^+ neurons, range 21 to 76, from N=42 mice). We counted FISH-labeled cells with DAPI-counterstained nuclei located in the RTN region within ~100 μm of the ventral medullary surface. We considered cells with at least 3 *Fos*-associated puncta as *Fos*-positive. Using these criteria, CO_2-activated RTN neurons were defined as *Fos*-expressing *Nmb*$^+$, DAPI-stained neurons and CO_2-activated astrocytes were defined as *Fos*-expressing *Aldh1l1*$^+$, DAPI-stained profiles. No stereological correction factor was applied. The investigator assessing and quantifying cellular profiles was blinded to treatment.

In vitro electrophysiology.

Brainstem slices were prepared essentially as described previously (Mulkey et al., 2004; Wang et al., 2013; Kumar et al., 2015; Shi et al., 2016). Briefly, neonatal mouse pups (P7–P11) were anesthetized with ketamine and xylazine (375 mg/kg and 25 mg/kg, i.m.) and brainstems were removed in ice-cold, sucrose-substituted solution, containing (mM): 260 sucrose, 3 KCl, 5 $MgCl_2$, 1 $CaCl_2$, 1.25 NaH_2PO_4, 26 $NaHCO_3$, 10 D-glucose, and 1 kynurenic acid. Slices were cut in the transverse plane (300 μm) with a microslicer (DSK 1500E; Dosaka) and incubated first for 20 min at 34°C in Ringer's solution containing (mM): 130 NaCl, 3 KCl, 2 $MgCl_2$, 2 $CaCl_2$, 1.25 NaH_2PO_4, 26 $NaHCO_3$, and 10 D-glucose. For labeling astrocytes, the Ringer's solution also included 0.5-1 μM sulforhodamine 101 (SR101, Sigma-Aldrich), and those slices were rinsed for a further 10 min at 34°C in that same solution without SR101. Slices were subsequently maintained in SR101-free Ringer's solution at room temperature and covered with aluminum foil until used for recording. All slicing and incubation solutions were pH 7.4 and bubbled with 95% O_2 and 5% CO_2.

Electrophysiological recordings were obtained in the RTN region of brainstem slices. Astrocytes were identified by their characteristic shape and size and labeling with SR101 dye (Nimmerjahn et al., 2004; Kafitz et al., 2008). RTN neurons were identified in slices from Phox2b-GFP mice by their location and GFP fluorescence (Lazarenko et al., 2009; Li et al., 2021). Slices were placed in a recording chamber mounted on a fluorescence microscope (Zeiss Axioskop FS) and bathed in HEPES-based solution containing (mM): 140 NaCl, 3 KCl, 2 $MgCl_2$, 2 $CaCl_2$, 10 HEPES, 10 D-glucose, pH 7.4. An NBCe1-mediated current was evoked by switching the bath solution to a HCO_3^--based Ringer's solution (as above, bubbled with 95% O_2 and 5% CO_2, pH 7.4). Tetrodotoxin (TTX, 1 uM; Bio-Techne Tocris, Minneapolis, MN) was added to the bath along with a cocktail of blockers (10 μM CNQX, 10 μM bicuculline, 30 μM strychnine; Sigma-Aldrich) to block receptors for fast excitatory (glutamate) and inhibitory transmitters (GABA, glycine). Patch electrodes (3–6 MΩ) were filled with pipette solution containing (mM): 120 KCH_3SO_3, 4 NaCl, 1 $MgCl_2$, 0.5 $CaCl_2$, 10 HEPES, 10 EGTA, 3 Mg-ATP, 0.3 GTP-Tris (pH 7.2, with KOH); electrode tips were coated with Sylgard 184 (Dow Corning). Whole cell and cell-attached voltage clamp recordings were obtained using pClamp, an Axopatch 200B amplifier, and a Digidata 1440A analog-to-digital converter (all from Molecular Devices, San Jose, CA). All

membrane voltages were corrected for a 10-mV liquid junction potential. Compensation for series resistance (60-70%) and cell capacitance was obtained using the amplifier circuits. The pH sensitivity of individual RTN neurons was assessed by measuring cell-attached firing responses in bicarbonate-based bath solutions bubbled with either 5% CO_2 (pH=7.4) or 10% CO_2 (pH=7.1) at a holding potential (Vh) of −60 mV (Perkins, 2006; Lazarenko et al., 2009; Li et al., 2021). In astrocytes, NBCe1-mediated current was quantified under voltage clamp at −60 mV as the outward current induced by changing from HEPES-based to CO_2/HCO_3^--based bath (at the same pH) that was sensitive to the specific NBCe1 blocker, S0859 (30 μM; Sigma-Aldrich; (Ch'en et al., 2008). The astrocytic input resistance and zero current potential (Em) were obtained from *I*-V curves (10 mV steps from from −110 to 30 mV, 100 ms, Vhold=−90 mV), the CO_2-induced inward current was measured (Vhold=−80 mV) during exchange of bath solutions equilibrated with 5% CO_2 and 10% CO_2 and used to calculate the shift in membrane potential.

Quantitative reverse transcriptase polymerase chain reaction (qRT-PCR).

Expression of NBCe1 and NBCe2 was determined in control and conditional knockout adult mice by qRT-PCR. The ventral medullary region encompassing the RTN was microdissected for RNA isolation from brainstem slices, prepared as above. We performed qRT-PCR using an iCycler iQ (Bio-Rad, USA) and Bio-Rad iQ SYBR Green Supermix in a 25 μl reaction volume from each sample in quadruplicate; each animal contributed a single data point for analysis (Cre^- mice, N=7; Cre^+ mice, N=5). We used the following primer sets for NBCe1 (*Slc4a4*: forward 5'-TTCAGGCTCTCTCTGCGATT-3' and reverse 5'-CTCAAGATGGTAAGCGGTTGA-3'), NBCe2 (*Slc4a5*: forward 5'-GCTCCGGGAGAGGGTCAGCT-3' and reverse 5'-CCGGGCAGAGCTTCGGTTCG-3') and GAPDH (*Gapdh*: forward 5'-GCAAATTCAACGGCACAGTCAAGG-3' and reverse 5'-TCTCGTGGTTCACACCCATCACAA-3'). Specificity of the primers was assessed by generating a melting curve of the PCR product and standard curve; PCR efficiencies were determined for primer pairs (92-100%). The protocol entailed: denaturation (95°C, 10 min.), amplification and quantification (42 cycles: 95°C, 20 s; 60°C, 20 s; 72°C, 20 s) and melt curve analysis (ramp from 55–95°C, 0.5°C increments for 2 s). Cycle threshold (Ct) levels were re-scaled by their average and transformed into relative quantities using the amplification efficiency, as described (Pfaffl, 2001). The Ct values of test genes were normalized to GAPDH, an internal reference gene (ΔCt = Ct(test) – Ct(GAPDH)).

Blood gas analysis.

Adult mice were habituated to a tail warmer and restraint apparatus (Braintree Scientific, Inc., Braintree, MA, USA) for 30 min one day before, and then for an additional 30 min immediately prior to blood sampling. For blood sampling, awake mice were gently restrained, and the tail was slightly warmed before arterial blood was collected from the ventral tail artery (~100 μl) into heparinized capillary tubes for immediate analysis using a handheld blood gas analyzer (iSTAT, with CG4+ cartridge, Abbott Point of Care Diagnostics, Princeton, NJ) (Kumar et al., 2015).

Statistics.

All statistical analyses were performed using GraphPad Prism (v. 7.04); details of specific tests are provided in the text or figure legends, and parametric tests were used when data were normally distributed (Shapiro-Wilk test). Data are presented in box and whiskers format (the median bisects a box bounded by the 25%ile and 75%ile, with whiskers depicting the range), or as mean ± standard deviation (sd). Statistical significance was set at $P<0.05$.

Results

We generated conditional knockout mice to test the role of astrocytic NBCe1 in the central respiratory chemoreflex. To eliminate NBCe1 expression in astrocytes, we obtained mice in which loxP sites surrounded the 12th exon of *Slc4a4* (Vairamani et al., 2018), the NBCe1 gene, and crossed those animals with GFAP-Cre or Aldh1l1-Cre/ERT2 mice in which Cre recombinase is expressed primarily in astrocytes in the CNS (Garcia et al., 2004; Winchenbach et al., 2016). We validated deletion of *Slc4a4* in astrocytes using histochemical, molecular and/or electrophysiological approaches, and then examined neuron/astrocyte activation (*Fos*) and ventilatory responses *in vivo* to raised CO_2 (hypercapnia) or lowered O_2 (hypoxia).

Astrocytic NBCe1 expression is reduced in GFAP-Cre conditional knockout mice.

We used multiplexed fluorescence *in situ* hybridization (FISH, by RNAscope) to examine *Slc4a4* expression in astrocytes (identified by their expression of *Aldh1l1*) within the RTN region of conditional knockout mice. As previously described, the RTN comprises a distinct cluster of neurons, defined in part by selective expression of *Nmb*, that reside between the facial motor nucleus and the ventral surface of the rostral medulla oblongata (Shi et al., 2017). In the region of *Nmb*-expressing RTN neurons from Cre-negative control animals (*Slc4a4*$^{f/f}$), we found robust expression of *Slc4a4* transcripts in *Aldh1l1*-expressing astrocytes (Fig. 1A). By contrast, in Cre-positive GFAP-Cre;*Slc4a4*$^{fl/fl}$ mice, *Slc4a4* expression was strongly reduced in *Aldh1l1*-expressing astrocytes (Fig. 1B); notably, *Slc4a4* depletion was observed most prominently in astrocytes located near the ventral medullary surface, while more dorsally located *Aldh1l1*-expressing astrocytes retained *Slc4a4* expression. This differential depletion of *Slc4a4* in ventral medullary surface astrocytes in GFAP-Cre mice appears to reflect differential expression of *Gfap*, which is often a marker of activated astrocytes and can be variably expressed among astrocytic populations, including preferentially at greater levels in surface astrocytes in the RTN region (see Fig. 5A) (Walz & Lang, 1998; Angelova et al., 2015; SheikhBahaei et al., 2018). We should also note that Cre expression has been reported in cells other than astrocytes in this GFAP-Cre mouse line (Jax#012886). However, since *Slc4a4* expression is largely localized to astrocytes in control mice (Theparambil et al., 2020), it is likely that any effects in these mice are due preferentially, if not exclusively, to deletion of *Slc4a4* from those cells.

The related NBCe2 transporter is prominently expressed in epithelium of the choroid plexus (Damkier et al., 2013; Christensen et al., 2018), but minimal *Slc4a5* expression is expected normally for astrocytes and neurons. Consistent with this, we found little evidence for

Slc4a5 expression in any cells within the RTN region; this was true for both Cre-negative and Cre-positive *Slc4a4*$^{fl/fl}$ mice, also suggesting no compensatory upregulation of NBCe2 expression after deletion of NBCe1 (Fig. 1C,D). Likewise, the strong *Slc4a5* expression observed in the choroid plexus was unaffected in Cre-positive mice (Fig. 1E,F).

To quantify deletion of *Slc4a4* in control and conditional knockout mice we also performed qRT-PCR using cDNA obtained from the RTN region that was microdissected from acute brain slices (Fig. 1G); we again also looked for any compensatory changes in *Slc4a5* expression. Consistent with the FISH results, levels of *Slc4a4* transcripts were significantly reduced in GFAP-Cre;*Slc4a4*$^{fl/fl}$ mice, by comparison to control *Slc4a4*$^{fl/fl}$ mice (by ~74%; $2^{-\Delta Ct}$ = 0.0066 ± 0.0040 vs. 0.0018 ± 0.0009 for Cre^{-} and Cre^{+}, N= 7 & 5 mice; P=0.0025, Mann-Whitney U-test), whereas *Slc4a5* expression was found at equally low levels in both control and conditional knockout mice ($2^{-\Delta Ct}$ = 0.0003 ± 0.0003 vs. 0.0003 ± 0.0002 for Cre^{-} and Cre^{+}, N= 6 & 5 mice; P=0.5368, Mann-Whitney U-test).

NBCe1 function is disrupted in astrocytes from GFAP-Cre conditional knockout mice.

We assessed NBCe1 function by recording from astrocytes in brain slices from control (*Slc4a4*$^{fl/fl}$) and conditional GFAP-Cre;*Slc4a4*$^{fl/fl}$ knockout mice. Astrocytes were identified in the RTN region by their distinctive size and shape, and their uptake of SR101 dye (Fig. 1H) (Nimmerjahn et al., 2004; Kafitz et al., 2008). In addition, by whole-cell voltage clamp recording, they presented with a characteristically linear current-voltage (*I*-V) relationship and zero-current potential near the predicted E_K (Fig. 1I). In slices from Cre^{-} control mice and Cre^{+} knockout mice, the input resistance (R_N) for all astrocytes recorded under resting condition was 31.2 ± 16.4 MΩ and 47.0 ± 29.7 MΩ and with a corresponding zero current potential of −94.5 ± 3.3 mV and −93.7 ± 3.5 mV (n=26 & 39 cells, N=5 & 10 mice). It should be noted that SR101 can label other cell types, especially at concentrations higher than we used here (Hulsmann et al., 2017). However, by targeting cells with these additional morphological features and characteristic membrane properties, along with the NBCe1-like currents described below, we believe this approach has appropriately identified the recorded cells as astrocytes.

In astrocytes from GFAP-Cre-negative control mice, exchanging the perfusate from a HEPES-based to a HCO_3^--based solution generated a robust outward current (Fig. 1J); this current reflected NBCe1-mediated HCO_3^- influx, at least in part, since it was strongly inhibited by the NBCe1-specific blocker, S0859 (30 μM; (Ch'en et al., 2008). As shown in Fig. 1K, the total HCO_3^--induced outward current was reduced in astrocytes from conditional NBCe1 knockout mice (180.0 ± 74.4 pA vs. 38.0 ± 32.9 pA for Cre^{-} vs. Cre^{+}, n= 10 & 13 cells, N=6 & 5 mice; P<0.0001, unpaired t-test), and the S0859-sensitive component of those diminished currents was essentially eliminated (accounting for 55.9 ± 19.0% vs. 2.1 ± 27.0% of HCO_3^--induced outward current in Cre^{-} and Cre^{+} mice, n=7 & 8 cells, N=6 & 5 mice; P=0.0007, unpaired t-test). Together, these data verify disrupted *Slc4a4* expression and NBCe1 function in ventral medullary astrocytes from GFAP-Cre conditional knockout mice.

CO_2- and hypoxia-stimulated breathing is unaffected by NBCe1 deletion in astrocytes from GFAP-Cre mice.

We used whole animal plethysmography to test ventilatory responses to CO_2 and hypoxia in control mice with intact NBCe1 and in GFAP-Cre-expressing littermates with deletion of NBCe1 in RTN-adjacent astrocytes (Fig. 2). Conscious mice were exposed to increasing concentrations of CO_2 in the inspired air, and with constant hyperoxia (60% O_2, balanced with N_2) to minimize effects of peripheral chemoreceptors and emphasize the centrally mediated respiratory chemoreflex (Basting et al., 2015). As evident in the exemplar respiratory flow traces and grouped data (Fig. 2A,B), the stimulatory effect of different levels of CO_2 on minute ventilation (V_E; ml/min/g) was indistinguishable between Cre^- and Cre^+ mice ($F_{4,110}$=0.1181, P=0.9758 for interaction, 2-way ANOVA, N=11 & 13), with no difference at the highest CO_2 tested (Δ V_E in 8% CO_2: 1.26 ± 0.27 ml/min/g vs. 1.35 ± 0.34 ml/min/g, N=11 and 13; P=0.5172, unpaired t-test). This reflected essentially identical CO_2-dependent effects on both respiratory frequency (fR, $F_{4,110}$=0.1654, P=0.9555 for interaction, 2-way ANOVA; Δ fR at 8% CO_2: 48.3 ± 24.6 breaths/min vs. 43.6 ± 29.6 breaths/min for Cre^- and Cre^+, N=11 & 13, P=0.6771, unpaired t-test) and tidal volume (V_T, $F_{4,110}$=0.01937, P=0.9993 for interaction, 2-way ANOVA; Δ V_T at 8% CO_2: 4.6 ± 1.5 μl/breath/g vs. 4.9 ± 1.5 μl/breath/g for Cre^- and Cre^+, N=11 & 13, P=0.6781, unpaired t-test). Thus, NBCe1 deletion from astrocytes had little overall effect on CO_2-stimulated breathing.

Hypoxia stimulates breathing via mechanisms that primarily involve actions on peripheral chemoreceptors, although recent work has suggested contributions from brainstem astrocytes in a central component of the hypoxia reflex (Angelova et al., 2015; Gourine & Funk, 2017). We found no difference in V_E between *Slc4a4*$^{fl/fl}$ mice and GFAP-Cre;*Slc4a4*$^{fl/fl}$ littermates (N=11 & 12) when exposed to either hyperoxic (60% O_2; 1.05 ± 0.29 ml/min/g vs. 1.08 ± 0.19 ml/min/g), normoxic (21% O_2; 1.04 ± 0.33 ml/min/g vs. 1.10 ± 0.15 ml/min/g) or hypoxic (10% O_2; 1.59 ± 0.38 ml/min/g vs. 1.76 ± 0.28 ml/min/g) gas mixtures (Fig. 2C; $F_{2,63}$=0.3825, P=0.6837 for interaction, 2-way ANOVA). In addition to stimulating ventilation, hypoxia also enhances the periodic generation of augmented breaths, or sighs. The number of sighs was increased during hypoxia exposure in both control Cre-negative *Slc4a4*$^{fl/fl}$ mice (from 1.0 ± 0.8 sighs/min to 4.9 ± 1.9 sighs/min, N=11) and their Cre-expressing GFAP-Cre;*Slc4a4*$^{fl/fl}$ littermates (from 1.0 ± 1.0 sighs/min to 5.8 ± 1.8 sighs/min, N=12), and there was no difference in the effect of hypoxia on sighs between genotypes (Fig. 2C; $F_{1,42}$=0.9778 for interaction, P=0.3284, 2-way ANOVA). These data indicate that astrocytic NBCe1 is not required for normal ventilatory responses to changes in inspired oxygen levels.

NBCe1 is not required for CO_2-mediated activation of RTN neurons or astrocytes.

We examined effects of GFAP-Cre-mediated NBCe1 deletion on CO_2-evoked activation of RTN neurons and local astrocytes using *Fos* expression as a surrogate for cellular activation *in vivo* (Fig. 3A,B). In both control and NBCe1 conditional knockouts, exposure to CO_2 (12% CO_2, 60% O_2, balance N_2) caused a robust stimulation of *Fos* expression by the majority of RTN neurons (Fig. 3C; $F_{1,17}$=335.4, P<0.0001, for CO_2 vs. hyperoxia, 2-way ANOVA). However, there was no genotype-dependent difference in the numbers

of CO_2-activated RTN neurons (Fig. 3C; $F_{1,17}$=0.02322, P=0.8807 for Cre^- vs. Cre^+, 2-way ANOVA). Specifically, we found *Fos*-labeling in 60.3 ± 2.2% of *Nmb*-expressing RTN neurons from Cre^- control mice (N=6) and in 61.1 ± 3.5% of those cells from Cre^+ conditional knockout mice (N=8). Likewise, CO_2 exposure induced *Fos* expression in *Aldh1l1*-expressing RTN astrocytes (Fig. 3D; $F_{1,17}$=28.84, P<0.0001, for CO_2 vs. hyperoxia, 2-way ANOVA), but again CO_2-evoked activation of astrocytes was not different between genotypes (number of *Aldh1l1*-expressing RTN-adjacent astrocytes from Cre^- mice: 22.0 ± 2.9, N=6; from Cre^+ mice: 20.0 ± 2.3, N=8; $F_{1,17}$=1.513, P=0.2355 for Cre^- vs. Cre^+, 2-way ANOVA).

We also tested whether NBCe1 is required for activation of RTN neurons and astrocytes by CO_2 *in vitro*. We performed cell-attached recordings of action potential firing from GFP-expressing RTN neurons in brainstem slices from Phox2b-GFP mice during exposure to 5% CO_2 (pH=7.4) and 10% CO_2 (pH=7.1), under control conditions and in the presence of S0859 (30 μM). As shown in Fig. 4A, we found no difference in firing rate under control conditions and in the presence of S0859 during exposure to either 5% CO_2 (1.9 ± 1.5 Hz vs. 1.7 ± 1.6 Hz) or 10% CO_2 (2.9 ± 1.8 Hz vs. 2.7 ± 1.6 Hz; n=10, N=6; $F_{1,18}$=0.09559 for control vs. S0859, P=0.7607, 2-way RM-ANOVA); under both conditions, CO_2 had essentially identical effects on RTN firing rate (ΔHz = 1.1 ± 0.6 Hz and 1.0 ± 0.5 Hz, for control vs. S0859; n=10, N=6; P=0.7730, paired t-test). In addition, we performed whole cell recordings of CO_2-induced current from RTN astrocytes in brainstem slices obtained from GFAP-Cre;*Slc4a4*$^{fl/fl}$ mice. A change from 5% CO_2 to 10% CO_2 in the perfusate consistently evoked an inward current in astrocytes from both Cre^- and Cre^+ mice (Fig. 4B), and although this CO_2-induced current appeared to trend toward smaller amplitudes in NBCe1-deleted astrocytes (Fig. 4C), the values were not significantly different between genotypes (63.3 ± 40.6 pA and 40.0 ± 32.8 pA, n=22 & 17, N=5 & 6; P=0.0673, Mann Whitney test). In addition, we also found no difference in effects of CO_2 on membrane potential calculated in those same cells from Cre^- and Cre^+ mice (Fig. 4C; 1.8 ± 1.6 mV and 1.9 ± 1.8 mV, P=0.7314, Mann Whitney test).

Together with the plethysmography results, these *in vivo* and *in vitro* data indicate that elimination of NBCe1 from GFAP-expressing astrocytes has no significant effect on activation of RTN neurons or astrocytes by CO_2 and does not alter the central respiratory chemoreflex.

Chemoreflex-stimulated breathing is retained when Slc4a4 is deleted broadly in astrocytes of Aldh1l1-Cre/ERT2 mice.

As described above, the floxed *Slc4a4* gene was effectively excised in ventral medullary astrocytes near the RTN using the GFAP-Cre mouse line, but *Slc4a4* expression was not eliminated in numerous other nearby astrocytes. This likely reflects elevated expression of *Gfap* that is restricted mainly to activated astrocytes (Walz & Lang, 1998; Angelova et al., 2015). Indeed, we find very high levels of *Gfap* transcripts in astrocytes in the vicinity of *Nmb*-expressing RTN neurons near the ventral medullary surface (SheikhBahaei et al., 2018) whereas *Gfap* was undetectable in many other astrocytes identified by *Aldh1l1* expression, a more broadly expressed marker (Fig. 5A).

Therefore, we sought to obtain more widespread astrocytic depletion of NBCe1 by using a mouse line with Cre expression driven from the *Aldh1l1* locus. In initial work, we were unable to obtain Cre^+ pups after crossing Aldh1l1-Cre mice with $Slc4a4^{fl/fl}$ animals, suggesting that early deletion of NBCe1 from astrocytes was not compatible with survival. However, we found we could use a tamoxifen-inducible Aldh1l1-Cre/ERT2 line to obtain Cre^- and Cre^+ littermates for successful deletion of *Slc4a4* by treating those adult animals with tamoxifen.

We verified Cre- and tamoxifen-dependent astrocyte deletion of *Slc4a4* in this mouse model by FISH, as shown in Fig. 5B–E. Specifically, *Slc4a4* expression was strongly reduced in *Aldh1l1*-expressing astrocytes of Cre-positive $Slc4a4^{fl/fl}$ mice that were treated with tamoxifen (Cre^+:T), by comparison to the three different control groups: Cre-negative mice treated with either vehicle or tamoxifen (Cre^-:V and Cre^-:T), or Cre-positive mice treated with vehicle (Cre^+:V). Unlike with the GFAP-Cre mice, depletion of *Slc4a4* expression in the RTN region in these Cre^+:T mice was not limited only to the astrocytes near the ventral medullary surface (cf. Fig. 5E and Fig. 1B), and indeed was much more widespread throughout the brainstem (*not shown*).

We examined the effects on breathing of chemoreceptor stimuli, both elevated CO_2 and variable O_2, in these inducible, conditional knockout mice. There was no difference in the peak stimulatory effect of CO_2 on breathing among the different experimental groups before or after vehicle or tamoxifen treatment (Fig. 6A; pre: $F_{3,27}$=0.5080, P=0.6801; post: $F_{3,27}$=2.069, P=0.1279, ANOVA). Although there was no difference in the stimulatory effect of increasing levels of CO_2 on V_E in the experimental groups post-treatment (Fig. 6B, *Inset*: $F_{12,135}$=0.8097, P=0.6401, for interaction by 2-way ANOVA) we did note a significantly higher overall V_E in the Cre-positive, tamoxifen-treated NBCe1 knockout mice across CO_2 levels ($F_{3,135}$=16.66, P<0.0001 for genotype-treatment by 2-way ANOVA); this was particularly apparent when the Cre^+:T response was compared to the 95% confidence interval of the combined V_E response to CO_2 for the three control groups (Fig. 6B). The higher V_E in Cre^+:T mice was largely due to differences in V_T. Thus, the V_T for Cre^+:T was elevated across the CO_2 range over the other three experimental groups, which were not different from each other ($F_{3,135}$=37.83, P<0.0001 for genotype-treatment by 2-way ANOVA; at least P<0.05 for Cre^+:T vs. each of the other groups at all CO_2 levels, Tukey's multiple comparison test); on the other hand, there were no differences in fR among the experimental groups at any CO_2 level ($F_{3,135}$=3.605, P<0.0152 for genotype-treatment by 2-way ANOVA; at least P>0.10 for Cre^+:T vs. each of the other groups at all CO_2 levels, Tukey's multiple comparison test). Likewise, there was no difference between any of the experimental groups in hypoxia-stimulated breathing before or after vehicle or tamoxifen treatment (Fig. 6C; pre: $F_{3,24}$=1.905, P=0.1557; post: $F_{3,21}$=2.104, P=0.1302, ANOVA), and the higher overall V_E response for the Cre^+:T conditional knockouts was again apparent by comparison to the three control groups (Fig. 6D; $F_{1,685}$=16.34, P=0.0001, for genotype-treatment by 2-way ANOVA). Finally, hypoxia-induced sighs were not different across any of the experimental groups, before or following vehicle/tamoxifen treatment (Fig. 6E; pre: $F_{3,48}$=0.2274, P=0.8769; post: $F_{3,42}$=1.038, P=0.3857, 2-way ANOVA). So, these ventilatory responses to CO_2 and hypoxia were unaltered by NBCe1 deletion even as the overall V_E was shifted to higher levels in Cre^+:T mice.

We again used *Fos* expression to examine the stimulatory effect of CO_2 on RTN neurons and surrounding astrocytes in mice after NBCe1 depletion from astrocytes. As illustrated in the exemplar photomicrographs from RNAscope FISH (Fig. 7A–D), CO_2-induced *Fos* expression was equally prominent in *Nmb*-expressing RTN neurons and *Aldh1l1*-expressing astrocytes after NBCe1 depletion (i.e., in Cre^+ mice treated with tamoxifen) as in the various control groups. This was borne out in quantitative cell counts, which revealed no significant differences among these groups in percentage of *Fos*-labeled RTN neurons (Fig. 7E; $F_{1,17}$=0.01331, P=0.9095 for interaction, 2-way ANOVA) or numbers of *Fos*-labeled astrocytes (Fig. 7F; $F_{1,17}$=8.114, P=0.0111, 2-way ANOVA; all pairwise comparisons non-significant by Šídák's post hoc test).

Thus, data with inducible, conditional *Slc4a4* knockout mice obtained with an Aldh1l1-Cre/ERT2 driver line indicate that even widespread depletion of astrocytic NBCe1 has no demonstrable effect on CO_2-mediated activation of RTN neurons or nearby astrocytes, and also no effect on respiratory reflexes evoked by raised CO_2 or lowered O_2. We nevertheless observed a higher overall V_E in these mice across those experimental conditions.

Metabolic acidosis is associated with deletion of Slc4a4 in kidneys of tamoxifen-treated Aldh1l1-CreERT2 mice

Considering the elevated V_E observed in the Aldh1l1-Cre/ERT2 line of conditional NBCe1 knockout mice we performed blood gas analysis from tail arteries of the control and *Slc4a4*-deleted littermates. These data suggested a partially compensated metabolic acidosis in the Cre^+, tamoxifen-treated mice, by comparison to all the other control groups (Table 1). That is, we observed that arterial pH was markedly acidotic in the conditional NBCe1 knockouts, relative to all controls (pH=7.21 ± 0.02, N=10 vs. 7.41 ± 0.14, N=32; P<0.0001, unpaired t-test), and this occurred in combination with reduced HCO_3^- (10.5 ± 0.7 mM, N=10 vs. 19.9 ± 0.7 mM, N=32; P<0.0001, unpaired t-test) and lower PCO_2 (25.7 ± 1.1 mmHg, N=8 vs. 31.1 ± 0.7 mmHg, N=30; P=0.0016, unpaired t-test). The respiratory compensation was observed in the elevated V_E post treatment for the NBCe1 knockouts (see Fig. 6B,D) and by comparing V_E of Cre^+:T mice to pooled data from the three control groups under normoxic conditions (1.2 ± 0.1 ml/min/g vs. 0.9 ± 0.1 ml/min/g, N=6 & 17; P=0.0164, unpaired t-test).

NBCe1 is an important component of acid-base control by the kidney. So, given the marked metabolic acidosis in these conditional knockout mice, we examined the kidney to determine if there was an effect on NBCe1 expression. Indeed, as shown in Fig. 8A–D, we confirmed that *Aldh1l1* is expressed in kidney (Krupenko, 2009) and, accordingly, we found that *Slc4a4* expression was eliminated from kidney in a Cre- and tamoxifen-dependent manner. Thus, we expect that deletion of NBCe1 from the kidney in Cre^+, tamoxifen-treated $Slc4a4^{fl/fl}$ mice interferes with proximal tubular reabsorption of HCO_3^- and results in the observed metabolic acidosis (Lee et al., 2022). Note that *Gfap* is not expressed in kidney, *Slc4a4* expression was preserved in kidneys of GFAP-Cre conditional knockout mice (Fig. 8E,F), and those animals did not show any signs of metabolic acidosis (Table 2).

Discussion

Chemosensitive astrocytes that respond to CO_2/H^+ have been implicated in control of breathing by brainstem RTN neurons, with various hypotheses advanced for mechanisms that couple astrocytic responses to enhanced RTN neuronal activity (Guyenet & Bayliss, 2015; Guyenet et al., 2019). A contribution from astrocytic NBCe1 has been deemed critical in a number of these proposed mechanisms (Erlichman et al., 2008; Guyenet & Bayliss, 2015; Turovsky et al., 2016; Marina et al., 2018; Guyenet et al., 2019). Our results from two different lines of conditional knockout mice, both with astrocytic deletion of *Slc4a4*, indicate that NBCe1 is not required for CO_2-mediated activation of either RTN neurons or ventral medullary astrocytes – and is also dispensable for CO_2-stimulated breathing. These data indicate that if astrocytes contribute to respiratory chemosensitivity, the mechanism must be able to function independently of contributions from NBCe1.

Limitations and caveats

It is difficult to be completely assured of either the cell selectivity or the degree of gene knockout in studies of conditional knockout mice. In this study, we used GFAP-Cre and Aldh1l1-Cre/ERT2 mouse lines to eliminate the NBCe1 gene, *Slc4a4*, in astrocytes. The possible concerns with Cre expression by other brain cells in these mice are allayed by the nearly exclusive astrocytic expression of *Slc4a4* in the brain (Theparambil et al., 2020). On the other hand, it is clear that astrocytes in different brain regions can be phenotypically distinct (Walz & Lang, 1998; SheikhBahaei et al., 2018; Theparambil et al., 2020; Lee et al., 2022) and we indeed found differential expression of *Gfap* and *Aldh1l1* in the RTN (and other regions of the brainstem). Accordingly, the Cre-mediated recombination driven by the cognate GFAP and Aldh1l1 promoters yielded distinct patterns of *Slc4a4* deletion in the two different mouse lines, with incomplete penetrance and chimeric residual expression. Nonetheless, we found that respiratory reflexes induced by CO_2 and hypoxia were unaffected in either line. In this respect, it is worth noting that that a recent study that used yet another inducible, astrocyte-selective NBCe1 knockout mouse line, based on GLAST-Cre/ERT2, also reported no deficits in CO_2-stimulated breathing (see supplemental data in (Hosford et al., 2022). As with our tamoxifen-inducible Aldh1l1-Cre/ERT2 line, *Slc4a4* was also deleted in adult GLAST-Cre/ERT2 mice (Hosford et al., 2022), such that both lines mitigated potential issues associated with developmental compensation. Thus, across multiple lines of mice with variable NBCe1 knockout across different astrocytic populations, the common observation was that the respiratory chemoreflexes were unaffected. Nonetheless, it remains a formal possibility that complete elimination of NBCe1 across all astrocytic populations might reveal some alteration in CO_2- or hypoxia-mediated breathing.

NBCe1 function in RTN astrocytes is dispensable for CO_2-stimulated breathing

The evidence to suggest an important role for NBCe1 in proton sensing by astrocytes for CO_2-mediated, astrocytic-dependent regulation of breathing has been reviewed previously (Mulkey & Wenker, 2011; Guyenet & Bayliss, 2015; Guyenet et al., 2019; Gourine & Dale, 2022). In short, NBCe1 activity is increased in ventral medullary astrocytes during CO_2-induced acidification, likely reflecting a combination of intracellular acidification and

membrane depolarization (Wenker et al., 2010; Mulkey & Wenker, 2011; Turovsky et al., 2016). Upon CO_2 entry into the cell, intracellular acidification promotes elevated NBCe1 activity to take up additional HCO_3^-, buffering those pH changes (Theparambil et al., 2014; Turovsky et al., 2016); in brainstem astrocytes, CO_2-induced changes in intracellular Ca^{2+} were strongly reduced by NBCe1 block with S0859 or in NBCe1 knockout mice (Turovsky et al., 2016). In addition, CO_2 can induce a membrane depolarization of astrocytes by inhibition of inwardly-rectifying K^+ current with pharmacological properties suggestive of the Kir4.1-Kir5.1 heteromeric channels (Wenker et al., 2010; Mulkey & Wenker, 2011); in turn, astrocytic depolarization can increase HCO_3^- influx by virtue of the electrogenic nature of the NBCe1 transporter, and this so-called depolarization-induced alkalization is a well-described feature of brain acid-base control by astrocytes (Grichtchenko & Chesler, 1994; Chesler, 2003). Our experiments with conditional knockout mice reinforce the conclusion that *Slc4a4* expression is indeed responsible for S0859-sensitive HCO_3^--induced currents in astrocytes.

Despite the demonstrated depletion of NBCe1 in astrocytes in the conditional knockout mice examined here, RTN neuronal activation (i.e., *Fos* expression) and ventilatory stimulation by CO_2 were unaffected. As mentioned (see Introduction), multiple non-exclusive mechanisms by which NBCe1 might contribute to astrocytic chemosensation and respiratory stimulation by RTN neurons have been proposed (Guyenet & Bayliss, 2015; Guyenet et al., 2019). In one conception, increased astrocytic NBCe1 activity accentuates extracellular acidification (Erlichman et al., 2008), and this serves to activate proton-sensing mechanisms on RTN neurons (Guyenet & Bayliss, 2015; Guyenet et al., 2019). In another, the elevated NBCe1 activity evoked by CO_2 in astrocytes initiates additional ion exchange mechanisms to raise intracellular Ca^{2+} and allow release of ATP (Turovsky et al., 2016); enhanced RTN neuronal activity follows either directly by actions of ATP on those neurons (Gourine et al., 2010), or indirectly by ATP-mediated decreases in local blood flow to further raise extracellular CO_2/H^+ (Hawkins et al., 2017). The present work suggests that the proposed NBCe1-dependent astrocytic mechanisms are dispensable for central respiratory chemosensitivity.

It is important to note that CO_2-evoked Fos expression was retained in NBCe1-depleted astrocytes, and thus our observations do not preclude a separate, NBCe1-*in*dependent mechanism for CO_2 activation of astrocytes and for their proposed contribution to respiratory chemosensitivity. For example, Kir-dependent membrane depolarization may promote some alternative mechanism for intracellular Ca^{2+} elevation to support vesicular release of ATP or other gliotransmitters (Wenker et al., 2010; Mulkey & Wenker, 2011). Alternatively, non-vesicular release mechanisms may also be relevant, such as CO_2-dependent carbamylation and activation of ATP-permeating connexons, as suggested previously (Huckstepp et al., 2010a; Huckstepp et al., 2010b). Additional mechanistic work is warranted to elucidate the molecular/cellular basis for proposed effects of astrocytes on the central respiratory chemoreflex.

NBCe1 function in astrocytes is not required for hypoxic ventilatory response or hypoxia-induced sighs

Hypoxia may also directly activate astrocytes (Angelova et al., 2015; Gourine & Funk, 2017). Indeed, hypoxic inhibition of mitochondrial respiration, via elevated levels of reactive oxygen species, can drive calcium transients and calcium-dependent release of ATP (Angelova et al., 2015; Gourine & Funk, 2017); activated astrocytes can also release PGE_2 (Howarth et al., 2017), which enhances sighs (Viemari et al., 2013; Koch et al., 2015). However, unlike for CO_2-induced activation of astrocytes (Turovsky et al., 2016), a role for NBCe1 in direct activation of astrocytes by hypoxia has not been proposed. In this respect, the direct hypoxia-induced activation of astrocytes and associated purinergic signaling has been suggested to contribute to a central hypoxia reflex that stimulates breathing (Angelova et al., 2015; Gourine & Funk, 2017). We find no effect of astrocytic NBCe1 deletion on hypoxia-stimulated breathing or sighs suggesting that NBCe1 does not play a role in hypoxia-activation of astrocytes for breathing control; however, this could also reflect a predominance of peripheral chemoreceptor actions for hypoxia-stimulated breathing under our experimental conditions.

Aldh1l1-Cre/ERT2-mediated NBCe1 deletion in kidney leads to partially compensated metabolic acidosis

We found that mice with Aldh1l1-Cre/ERT2-mediated NBCe1 deletion displayed a partially compensated metabolic acidosis, with reduced PCO_2 and elevated overall ventilation. This appears to reflect loss of NBCe1 and reduced bicarbonate reabsorption from the kidney because we verified that *Aldh1l1* is expressed in kidney (Krupenko, 2009) and showed that *Slc4a4* expression was strongly reduced in Cre^+, tamoxifen-treated $Slc4a4^{fl/fl}$ mice. Despite this chronic metabolic acidosis, which might itself have blunted the hypercapnic ventilatory response, we found no difference in CO_2-stimulated breathing in those mice. In addition, there was no concomitant loss of *Slc4a4* expression in the kidneys of GFAP-Cre mice, which presented neither metabolic acidosis nor changes in baseline or CO_2-stimulated ventilation. Thus, it seems unlikely that effects on kidney account for the lack of effect on CO_2-stimulated breathing following NBCe1 knockout in these two different conditional knockout lines.

In conclusion, *Slc4a4* expression and NBCe1 function in astrocytes do not contribute appreciably to CO_2-stimulated (or hypoxia-evoked) breathing reflexes in mice. The mechanisms by which astrocytes contribute to the central respiratory chemoreflex remain to be elucidated, and our work indicates that they must be independent of previously proposed hypotheses that invoked local acidification or paracrine purinergic signaling dependent on astrocytic NBCe1 expression and function (Turovsky et al., 2016; Marina et al., 2018).

Supplementary Material

Refer to Web version on PubMed Central for supplementary material.

Acknowledgements and funding

The floxed *Slc4a4* mouse line was graciously provided by Dr. Gary E. Shull (Department of Molecular Genetics, Biochemistry and Microbiology, University of Cincinnati, Cincinnati, OH, USA). This study was funded by the National Institutes of Health (HL074011, to PGG; HL148004, to SBGA; HL061974 to GES; HL108609, to DAB); and the Center for Clinical and Translational Science and Training, and a Research Innovation Seed Grant from the University of Cincinnati (to GES). ECG was supported by T32 GM007055 and F31 HL154660.

Biography

Keyong Li received his PhD in Medical Neurobiology from Fudan University, Shanghai, China. He undertook postdoctoral training in the Department of Neuroscience, Cell Biology and Physiology at Wright State University before moving to the Department of Pharmacology at the University of Virginia as a research scientist. He is currently investigating different ion channels in neurons and astrocytes that are involved in central respiratory control during development, physiological challenge, and disease conditions.

Data availability statement

The datasets generated during the current study are available from the corresponding author on reasonable request.

References

Angelova PR, Kasymov V, Christie I, Sheikhbahaei S, Turovsky E, Marina N, Korsak A, Zwicker J, Teschemacher AG, Ackland GL, Funk GD, Kasparov S, Abramov AY & Gourine AV. (2015). Functional oxygen sensitivity of astrocytes. J Neurosci 35, 10460–10473. [PubMed: 26203141]

Basting TM, Burke PG, Kanbar R, Viar KE, Stornetta DS, Stornetta RL & Guyenet PG. (2015). Hypoxia silences retrotrapezoid nucleus respiratory chemoreceptors via alkalosis. J Neurosci 35, 527–543. [PubMed: 25589748]

Ch'en FF, Villafuerte FC, Swietach P, Cobden PM & Vaughan-Jones RD. (2008). S0859, an N-cyanosulphonamide inhibitor of sodium-bicarbonate cotransport in the heart. Br J Pharmacol 153, 972–982. [PubMed: 18204485]

Chesler M (2003). Regulation and modulation of pH in the brain. Physiol Rev 83, 1183–1221. [PubMed: 14506304]

Christensen HL, Barbuskaite D, Rojek A, Malte H, Christensen IB, Fuchtbauer AC, Fuchtbauer EM, Wang T, Praetorius J & Damkier HH. (2018). The choroid plexus sodium-bicarbonate cotransporter NBCe2 regulates mouse cerebrospinal fluid pH. J Physiol 596, 4709–4728. [PubMed: 29956324]

Damkier HH, Brown PD & Praetorius J. (2013). Cerebrospinal fluid secretion by the choroid plexus. Physiol Rev 93, 1847–1892. [PubMed: 24137023]

Del Negro CA, Funk GD & Feldman JL. (2018). Breathing matters. Nat Rev Neurosci 19, 351–367. [PubMed: 29740175]

Erlichman JS, Putnam RW & Leiter JC. (2008). Glial modulation of CO2 chemosensory excitability in the retrotrapezoid nucleus of rodents. Adv Exp Med Biol 605, 317–321. [PubMed: 18085292]

Garcia AD, Doan NB, Imura T, Bush TG & Sofroniew MV. (2004). GFAP-expressing progenitors are the principal source of constitutive neurogenesis in adult mouse forebrain. Nat Neurosci 7, 1233–1241. [PubMed: 15494728]

Gestreau C, Heitzmann D, Thomas J, Dubreuil V, Bandulik S, Reichold M, Bendahhou S, Pierson P, Sterner C, Peyronnet-Roux J, Benfriha C, Tegtmeier I, Ehnes H, Georgieff M, Lesage F, Brunet JF, Goridis C, Warth R & Barhanin J. (2010). Task2 potassium channels set central respiratory CO2 and O2 sensitivity. Proc Natl Acad Sci U S A 107, 2325–2330. [PubMed: 20133877]

Gourine AV & Dale N. (2022). Brain H(+) /CO(2) sensing and control by glial cells. Glia 70, 1520–1535. [PubMed: 35102601]

Gourine AV & Funk GD. (2017). On the existence of a central respiratory oxygen sensor. J Appl Physiol (1985) 123, 1344–1349. [PubMed: 28522760]

Gourine AV, Kasymov V, Marina N, Tang F, Figueiredo MF, Lane S, Teschemacher AG, Spyer KM, Deisseroth K & Kasparov S. (2010). Astrocytes control breathing through pH-dependent release of ATP. Science 329, 571–575. [PubMed: 20647426]

Grichtchenko II & Chesler M (1994). Depolarization-induced alkalinization of astrocytes in gliotic hippocampal slices. Neuroscience 62, 1071–1078. [PubMed: 7845587]

Guyenet PG & Bayliss DA. (2015). Neural control of breathing and CO2 homeostasis. Neuron 87, 946–961. [PubMed: 26335642]

Guyenet PG, Stornetta RL, Souza G, Abbott SBG, Shi Y & Bayliss DA. (2019). The Retrotrapezoid Nucleus: Central Chemoreceptor and Regulator of Breathing Automaticity. Trends Neurosci 42, 807–824. [PubMed: 31635852]

Hawkins VE, Takakura AC, Trinh A, Malheiros-Lima MR, Cleary CM, Wenker IC, Dubreuil T, Rodriguez EM, Nelson MT, Moreira TS & Mulkey DK. (2017). Purinergic regulation of vascular tone in the retrotrapezoid nucleus is specialized to support the drive to breathe. Elife 6.

Hodges MR & Richerson GB. (2010). Medullary serotonin neurons and their roles in central respiratory chemoreception. Respir Physiol Neurobiol 173, 256–263. [PubMed: 20226279]

Hosford PS, Wells JA, Nizari S, Christie IN, Theparambil SM, Castro PA, Hadjihambi A, Barros LF, Ruminot I, Lythgoe MF & Gourine AV. (2022). CO2 signaling mediates neurovascular coupling in the cerebral cortex. Nat Commun 13, 2125. [PubMed: 35440557]

Howarth C, Sutherland B, Choi HB, Martin C, Lind BL, Khennouf L, LeDue JM, Pakan JM, Ko RW, Ellis-Davies G, Lauritzen M, Sibson NR, Buchan AM & MacVicar BA. (2017). A Critical Role for Astrocytes in Hypercapnic Vasodilation in Brain. J Neurosci 37, 2403–2414. [PubMed: 28137973]

Huckstepp RT, Eason R, Sachdev A & Dale N. (2010a). CO2-dependent opening of connexin 26 and related beta connexins. J Physiol 588, 3921–3931. [PubMed: 20736419]

Huckstepp RT, id Bihi R, Eason R, Spyer KM, Dicke N, Willecke K, Marina N, Gourine AV & Dale N. (2010b). Connexin hemichannel-mediated CO2-dependent release of ATP in the medulla oblongata contributes to central respiratory chemosensitivity. J Physiol 588, 3901–3920. [PubMed: 20736421]

Hulsmann S, Hagos L, Heuer H & Schnell C. (2017). Limitations of Sulforhodamine 101 for Brain Imaging. Front Cell Neurosci 11, 44. [PubMed: 28293173]

Kafitz KW, Meier SD, Stephan J & Rose CR. (2008). Developmental profile and properties of sulforhodamine 101--Labeled glial cells in acute brain slices of rat hippocampus. J Neurosci Methods 169, 84–92. [PubMed: 18187203]

Koch H, Caughie C, Elsen FP, Doi A, Garcia AJ 3rd, Zanella S & Ramirez JM. (2015). Prostaglandin E2 differentially modulates the central control of eupnoea, sighs and gasping in mice. J Physiol 593, 305–319. [PubMed: 25556802]

Krupenko SA. (2009). FDH: an aldehyde dehydrogenase fusion enzyme in folate metabolism. Chem Biol Interact 178, 84–93. [PubMed: 18848533]

Kumar NN, Velic A, Soliz J, Shi Y, Li K, Wang S, Weaver JL, Sen J, Abbott SB, Lazarenko RM, Ludwig MG, Perez-Reyes E, Mohebbi N, Bettoni C, Gassmann M, Suply T, Seuwen K, Guyenet PG, Wagner CA & Bayliss DA. (2015). Regulation of breathing by CO(2) requires the proton-activated receptor GPR4 in retrotrapezoid nucleus neurons. Science 348, 1255–1260. [PubMed: 26068853]

Lazarenko RM, Milner TA, Depuy SD, Stornetta RL, West GH, Kievits JA, Bayliss DA & Guyenet PG. (2009). Acid sensitivity and ultrastructure of the retrotrapezoid nucleus in Phox2b-EGFP transgenic mice. J Comp Neurol 517, 69–86. [PubMed: 19711410]

Lee HW, Verlander JW, Shull GE, Harris AN & Weiner ID. (2022). Acid-base effects of combined renal deletion of NBCe1-A and NBCe1-B. Am J Physiol Renal Physiol 322, F208–F224. [PubMed: 35001662]

Li K, Abbott SBG, Shi Y, Eggan P, Gonye EC & Bayliss DA. (2021). TRPM4 mediates a subthreshold membrane potential oscillation in respiratory chemoreceptor neurons that drives pacemaker firing and breathing. Cell Rep 34, 108714. [PubMed: 33535052]

Loria CJ, Stevens AM, Crummy E, Casadesus G, Jacono FJ, Dick TE & Siegel RE. (2013). Respiratory and behavioral dysfunction following loss of the GABAA receptor alpha4 subunit. Brain Behav 3, 104–113. [PubMed: 23533098]

Marina N, Turovsky E, Christie IN, Hosford PS, Hadjihambi A, Korsak A, Ang R, Mastitskaya S, Sheikhbahaei S, Theparambil SM & Gourine AV. (2018). Brain metabolic sensing and metabolic signaling at the level of an astrocyte. Glia 66, 1185–1199. [PubMed: 29274121]

Meigh L, Greenhalgh SA, Rodgers TL, Cann MJ, Roper DI & Dale N. (2013). CO(2)directly modulates connexin 26 by formation of carbamate bridges between subunits. Elife 2, e01213. [PubMed: 24220509]

Mulkey DK, Stornetta RL, Weston MC, Simmons JR, Parker A, Bayliss DA & Guyenet PG. (2004). Respiratory control by ventral surface chemoreceptor neurons in rats. Nat Neurosci 7, 1360–1369. [PubMed: 15558061]

Mulkey DK & Wenker IC. (2011). Astrocyte chemoreceptors: mechanisms of H+ sensing by astrocytes in the retrotrapezoid nucleus and their possible contribution to respiratory drive. Exp Physiol 96, 400–406. [PubMed: 21169332]

Nimmerjahn A, Kirchhoff F, Kerr JN & Helmchen F. (2004). Sulforhodamine 101 as a specific marker of astroglia in the neocortex in vivo. Nat Methods 1, 31–37. [PubMed: 15782150]

Percie du Sert N, Hurst V, Ahluwalia A, Alam S, Avey MT, Baker M, Browne WJ, Clark A, Cuthill IC, Dirnagl U, Emerson M, Garner P, Holgate ST, Howells DW, Karp NA, Lazic SE, Lidster K, MacCallum CJ, Macleod M, Pearl EJ, Petersen OH, Rawle F, Reynolds P, Rooney K, Sena ES, Silberberg SD, Steckler T & Wurbel H. (2020). The ARRIVE guidelines 2.0: updated guidelines for reporting animal research. J Physiol 598, 3793–3801. [PubMed: 32666574]

Perkins KL. (2006). Cell-attached voltage-clamp and current-clamp recording and stimulation techniques in brain slices. J Neurosci Methods 154, 1–18. [PubMed: 16554092]

Pfaffl MW. (2001). A new mathematical model for relative quantification in real-time RT-PCR. Nucleic Acids Res 29, e45. [PubMed: 11328886]

SheikhBahaei S, Morris B, Collina J, Anjum S, Znati S, Gamarra J, Zhang R, Gourine AV & Smith JC. (2018). Morphometric analysis of astrocytes in brainstem respiratory regions. J Comp Neurol 526, 2032–2047. [PubMed: 29888789]

Shi Y, Abe C, Holloway BB, Shu S, Kumar NN, Weaver JL, Sen J, Perez-Reyes E, Stornetta RL, Guyenet PG & Bayliss DA. (2016). Nalcn Is a “Leak” Sodium Channel That Regulates Excitability of Brainstem Chemosensory Neurons and Breathing. J Neurosci 36, 8174–8187. [PubMed: 27488637]

Shi Y, Stornetta RL, Stornetta DS, Onengut-Gumuscu S, Farber EA, Turner SD, Guyenet PG & Bayliss DA. (2017). Neuromedin B Expression Defines the Mouse Retrotrapezoid Nucleus. J Neurosci 37, 11744–11757. [PubMed: 29066557]

Souza G, Kanbar R, Stornetta DS, Abbott SBG, Stornetta RL & Guyenet PG. (2018). Breathing regulation and blood gas homeostasis after near complete lesions of the retrotrapezoid nucleus in adult rats. J Physiol 596, 2521–2545. [PubMed: 29667182]

Theparambil SM, Hosford PS, Ruminot I, Kopach O, Reynolds JR, Sandoval PY, Rusakov DA, Barros LF & Gourine AV. (2020). Astrocytes regulate brain extracellular pH via a neuronal activity-dependent bicarbonate shuttle. Nat Commun 11, 5073. [PubMed: 33033238]

Theparambil SM, Naoshin Z, Defren S, Schmaelzle J, Weber T, Schneider HP & Deitmer JW. (2017). Bicarbonate sensing in mouse cortical astrocytes during extracellular acid/base disturbances. J Physiol 595, 2569–2585. [PubMed: 27981578]

Theparambil SM, Ruminot I, Schneider HP, Shull GE & Deitmer JW. (2014). The electrogenic sodium bicarbonate cotransporter NBCe1 is a high-affinity bicarbonate carrier in cortical astrocytes. J Neurosci 34, 1148–1157. [PubMed: 24453308]

Turovsky E, Theparambil SM, Kasymov V, Deitmer JW, Del Arroyo AG, Ackland GL, Corneveaux JJ, Allen AN, Huentelman MJ, Kasparov S, Marina N & Gourine AV. (2016). Mechanisms of CO2/H+ Sensitivity of Astrocytes. J Neurosci 36, 10750–10758. [PubMed: 27798130]

Vairamani K, Prasad V, Wang Y, Huang W, Chen Y, Medvedovic M, Lorenz JN & Shull GE. (2018). NBCe1 Na(+)-HCO3(−) cotransporter ablation causes reduced apoptosis following cardiac ischemia-reperfusion injury in vivo. World J Cardiol 10, 97–109. [PubMed: 30344957]

Viemari JC, Garcia AJ 3rd, Doi A, Elsen G & Ramirez JM. (2013). beta-Noradrenergic receptor activation specifically modulates the generation of sighs in vivo and in vitro. Front Neural Circuits 7, 179. [PubMed: 24273495]

Walz W & Lang MK. (1998). Immunocytochemical evidence for a distinct GFAP-negative subpopulation of astrocytes in the adult rat hippocampus. Neurosci Lett 257, 127–130. [PubMed: 9870336]

Wang S, Benamer N, Zanella S, Kumar NN, Shi Y, Bevengut M, Penton D, Guyenet PG, Lesage F, Gestreau C, Barhanin J & Bayliss DA. (2013). TASK-2 channels contribute to pH sensitivity of retrotrapezoid nucleus chemoreceptor neurons. J Neurosci 33, 16033–16044. [PubMed: 24107938]

Wenker IC, Kreneisz O, Nishiyama A & Mulkey DK. (2010). Astrocytes in the retrotrapezoid nucleus sense H+ by inhibition of a Kir4.1-Kir5.1-like current and may contribute to chemoreception by a purinergic mechanism. J Neurophysiol 104, 3042–3052. [PubMed: 20926613]

Winchenbach J, Duking T, Berghoff SA, Stumpf SK, Hulsmann S, Nave KA & Saher G. (2016). Inducible targeting of CNS astrocytes in Aldh1l1-CreERT2 BAC transgenic mice. F1000Res 5, 2934. [PubMed: 28149504]

KEY POINTS

- The electrogenic NBCe1 transporter is proposed to mediate local astrocytic CO_2/H^+ sensing that enables excitatory modulation of nearby retrotrapezoid nucleus (RTN) neurons to support chemosensory control of breathing.
- We used two different Cre mouse lines for cell-specific and/or temporally regulated deletion of the NBCe1 gene (*Slc4a4*) in astrocytes to test this hypothesis.
- In both mouse lines, *Slc4a4* was depleted from RTN-associated astrocytes but CO_2-induced *Fos* expression (i.e., cell activation) in RTN neurons and local astrocytes was intact.
- Likewise, respiratory chemoreflexes evoked by changes in CO_2 or O_2 were unaffected by loss of astrocytic *Slc4a4*.
- These data do not support the previously proposed role for NBCe1 in respiratory chemosensitivity mediated by astrocytes.

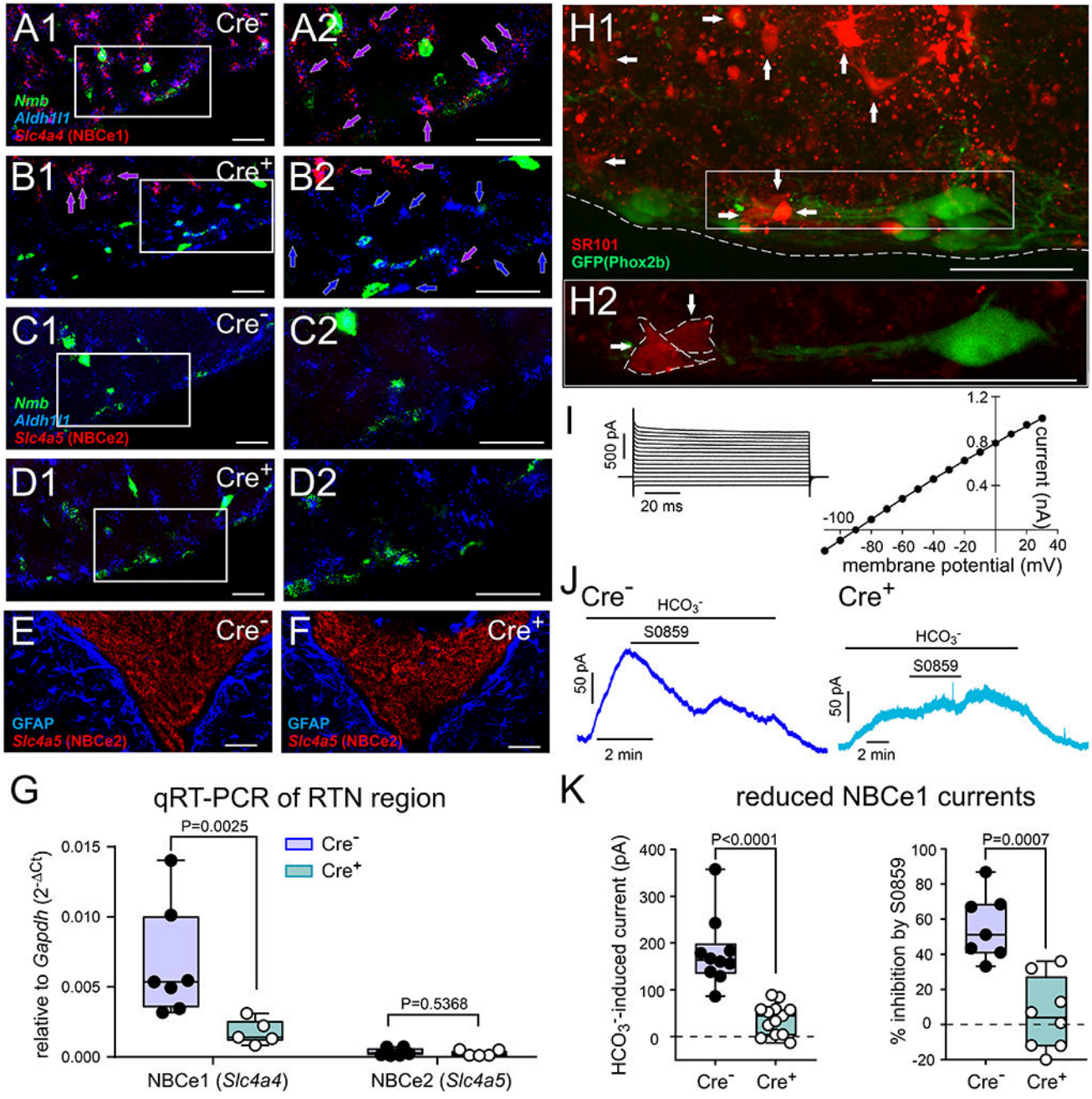

Figure 1. NBCe1 expression and current in ventral medullary astrocytes near RTN neurons in GFAP-Cre;*Slc4a4*$^{fl/fl}$ mice with no compensatory change in NBCe2 expression.

A-D. RNAscope for *Nmb* (RTN neurons), *Aldh1l1* (astrocytes) and either *Slc4a4* (**A,B**; NBCe1) or *Slc4a5* (**C,D**; NBCe2) on brainstem sections from Cre-negative (**A,C**) and Cre-positive (**B,D**) GFAP-Cre;*Slc4a4*$^{fl/fl}$ mice. Arrows indicate cells expressing: purple, *Aldh1l1/Slc4a4*; blue, *Aldh1l1*. Sections at ~−6.48 mm, relative to bregma; scale bars: 50 μm. Representative of N=10 & 11 mice.

E,F. RNAscope for *Slc4a5* (NBCe2) in choroid plexus from Cre-negative (**E**) and Cre-positive (**F**) GFAP-Cre;*Slc4a4*$^{fl/fl}$ mice. Sections at ~−6.48 mm, relative to bregma; scale bars: 50 μm. Representative of N=4 mice each.

G. qRT-PCR from microdissected RTN region quantifying expression of *Slc4a4* (NBCe1) or *Slc4a5* (NBCe2) in Cre-negative and Cre-positive GFAP-Cre;*Slc4a4*$^{fl/fl}$ mice. (NBCe1: P=0.0025 for Cre^- vs. Cre^+, N=7 & 5 mice: NBCe2: P=0.5368 for Cre^- vs. Cre^+, N=6 & 5 mice; by Mann-Whitney U-test)

H. Confocal images of SR101-labeled cells (*arrows*) among GFP-labeled RTN neurons in brain slices from Phox2b::GFP mice, shown in a Z-stack (**H1**) and at a single Z-plane (**H2**). Scale bar = 50 μm.

I. Exemplar whole cell voltage clamp recording of baseline *I*-V characteristics from an SR101-labeled astrocyte.

J. Whole cell current (V_{hold}=−80 mV) sensitive to the NBCe1 blocker (S0859, 30 μM) was assessed after switching from HEPES- to bicarbonate-based buffer in SR101-labeled astrocytes in the RTN region of brain slices from Cre-negative (*left*) and Cre-positive (*right*) GFAP-Cre;*Slc4a4*$^{fl/fl}$ mice.

K. Total HCO_3^--induced current (*left*; P<0.0001 for Cre^- vs. Cre^+ by unpaired t-test, n=10 & 13 cells) and S0859-sensitive current (*right*; P=0.0007 for Cre^- vs. Cre^+ by unpaired t-test, n=7 & 8 cells) in SR101-labeled RTN astrocytes from Cre^- and Cre^+ GFAP-Cre;*Slc4a4*$^{fl/fl}$ mice (N=6 & 5 mice).

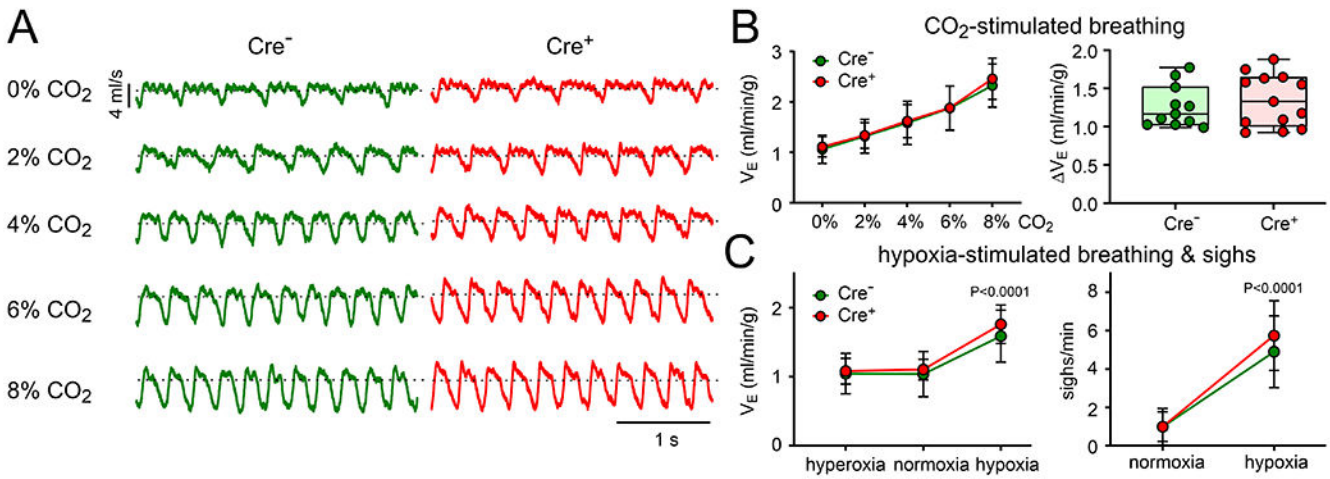

Figure 2. Effects of CO_2 and O_2 on minute ventilation and sigh frequency are unaffected by NBCe1 deletion from astrocytes in GFAP-Cre;*Slc4a4*$^{fl/fl}$ mice.

A. Whole body plethysmography recordings from unanesthetized Cre-negative and Cre-positive GFAP-Cre;*Slc4a4*$^{fl/fl}$ mice at increasing levels of inspired CO_2 (in 60% O_2, balance N_2). Dashed line shows approximate inspiratory-expiratory transition.

B. Effects of increasing inspired CO_2 (from 0% to 8%; 60% O_2, balance N_2) on minute ventilation (*left*; mean ± SD; $F_{4,110}$=0.1181, P=0.9758 for interaction, by 2-way ANOVA) and the change in V_E evoked by 8% CO_2 (*right*; P=0.5172, by unpaired t-test) were not different in Cre-negative and Cre-positive GFAP-Cre;*Slc4a4*$^{fl/fl}$ mice (N=11 and 13 mice).

C. Effects of hyperoxia (60% O_2, balance N_2) and hypoxia (10% O_2, balance N_2) on minute ventilation (*left*; mean ± SD; $F_{2,63}$=0.3825, P=0.6837 for interaction, by 2-way ANOVA) and frequency of hypoxia-induced sighs (*right*; mean ± SD; $F_{1,42}$=0.9778, P=0.3284 for interaction, by 2-way ANOVA) in Cre-negative and Cre-positive GFAP-Cre;*Slc4a4*$^{fl/fl}$ mice (N=11 and 12 mice, respectively).

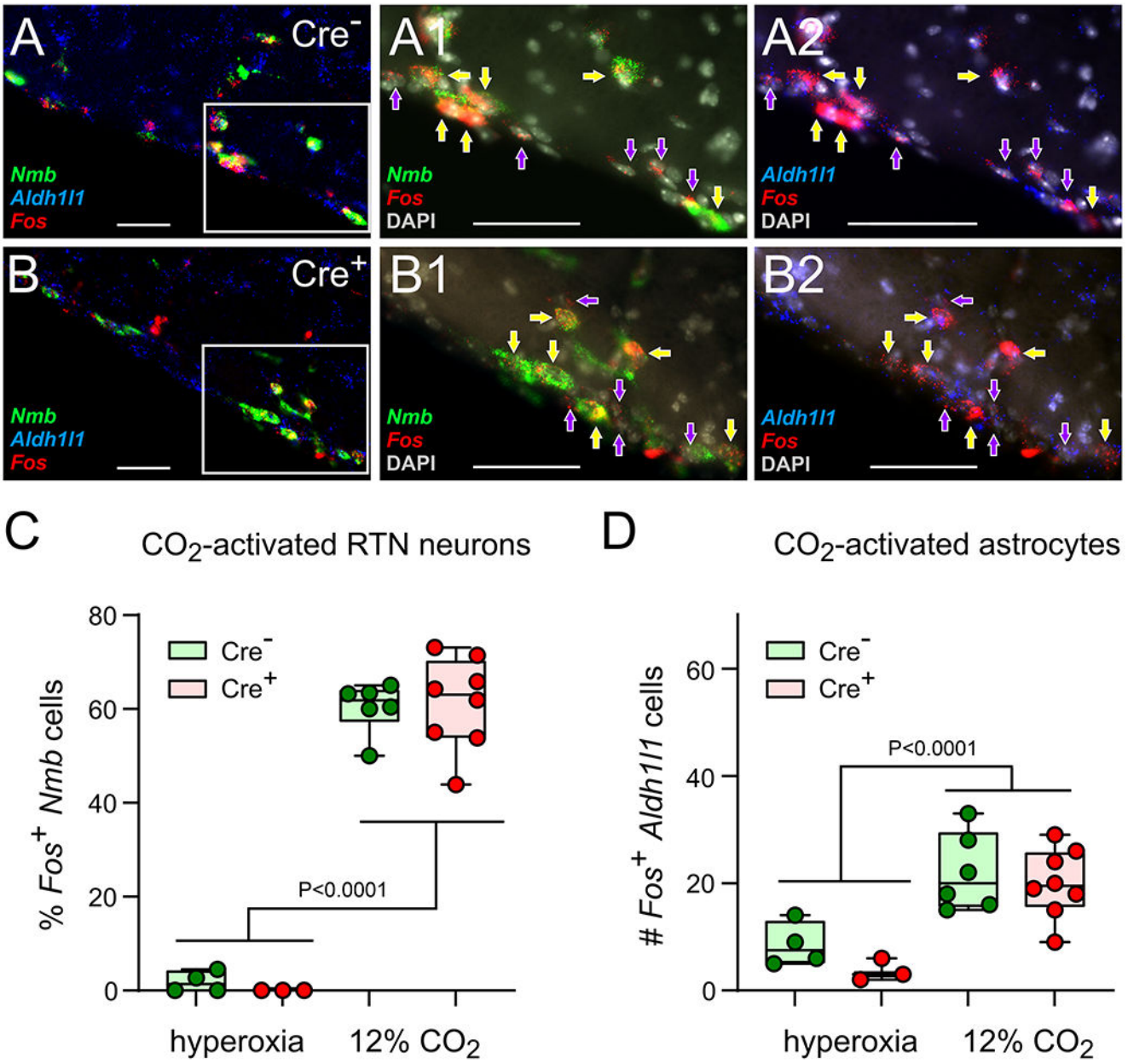

Figure 3. CO_2-stimulated Fos expression in the RTN region of GFAP-Cre;*Slc4a4*$^{fl/fl}$ mice.

A,B. RNAscope for *Nmb*, *Aldh1l1* and *Fos* (as indicated) in DAPI-stained brainstem sections from Cre-negative (**A**) and Cre-positive (**B**) GFAP-Cre;*Slc4a4*$^{fl/fl}$ mice after exposure *in vivo* to 12% CO_2 (60% O_2, balance N_2). Arrows indicate cells expressing: yellow, *Nmb/Fos*; purple, *Aldh1l1*/*Fos*. Sections at ~−6.48 mm, relative to bregma; scale bars: 50 μm.

C,D. Quantification of *Fos*$^+$ RTN neurons (**C**, *Nmb*$^+$ cells) and nearby *Fos*$^+$ astrocytes (**D**, *Aldh1l1*$^+$ cells) in the RTN region of Cre$^-$ and Cre$^+$ GFAP-Cre;*Slc4a4*$^{fl/fl}$ mice under control conditions (hyperoxia; 60% O_2, balance N_2; sections from N=4 & 3 mice, 30.5 ± 7.2 & 39.0 ± 2.0 Nmb$^+$ neurons) and after exposure to 12% CO_2 (60% O_2, balance N_2; sections

from N=6 & 8 mice, 49.2 ± 9.2 & 53.9 ± 10.0 Nmb^+ neurons). CO_2-induced Fos for Cre^- vs. Cre^+ by unpaired t-test: RTN neurons, P=0.5171; astrocytes, P= 0.3837.

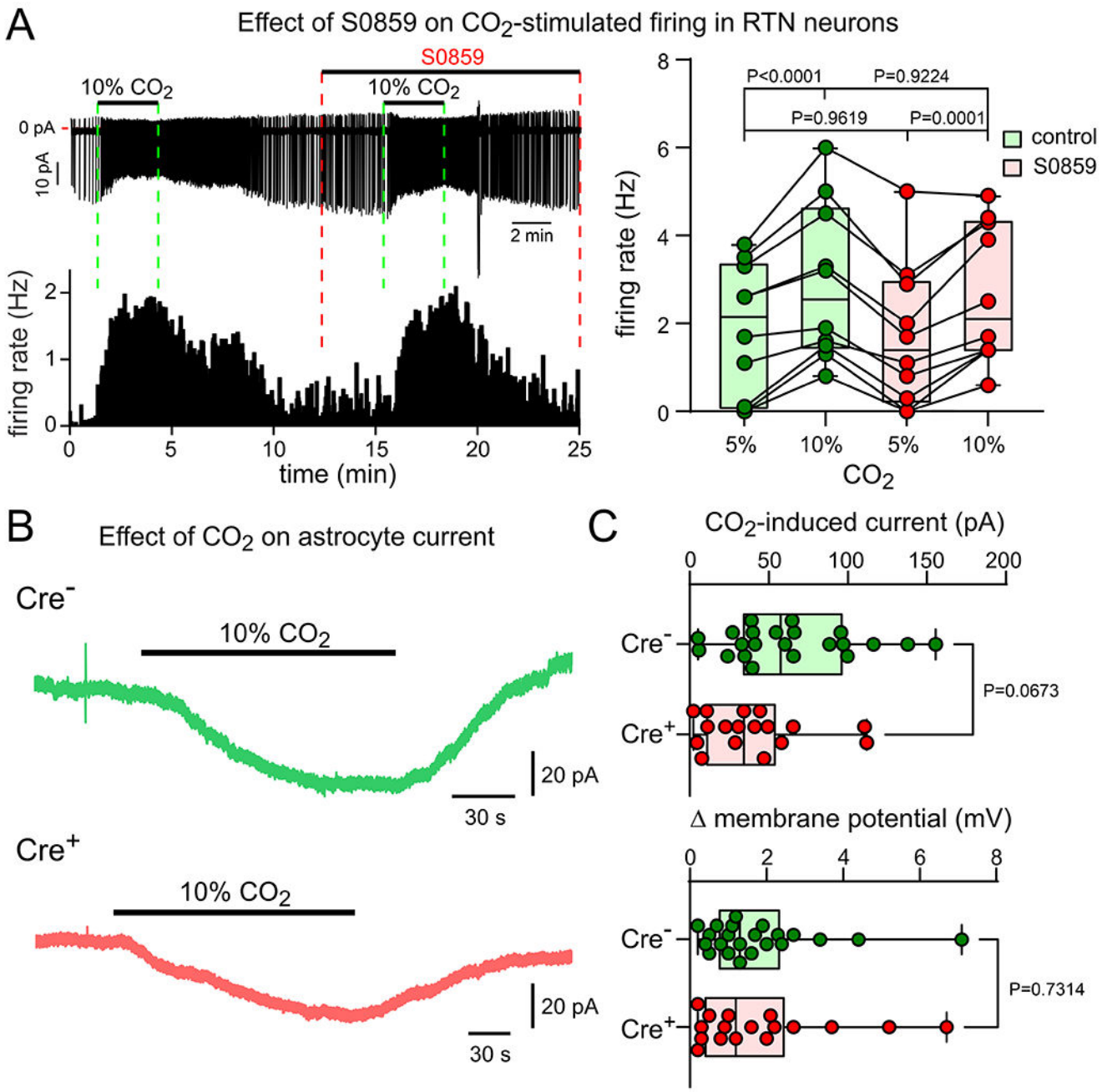

Figure 4. Effects of CO_2 on RTN neurons and astrocytes after blocking NBCe1 or deleting *Slc4a4* in astrocytes.

A. *Left*: Effect of CO_2 on action potential firing rate in an individual RTN neuron in a brainstem slice from a Phox2b::GFP mice, tested under control conditions and after blocking NBCe1 with S0859 (30 μM). *Right*: Summary data (n=10 cells, N=6 mice) shows that firing rate was increased by CO_2 in both conditions ($F_{1,18}$=58.75 for CO_2, P<0.0001, by 2-way ANOVA), but there was no effect of S0859 on firing rate in either 5% CO_2 or 10% CO_2 ($F_{1,18}$=0.09559 for S0859, P=0.7607). **B**. Exemplar records of CO_2-induced current in astrocytes from Cre-negative (*upper*) and Cre-positive (*lower*) GFAP-Cre;*Slc4a4*$^{fl/fl}$ mice.

C. Summary data reveals no significant difference in CO_2-induced current or membrane depolarization from control and NBCe1-deleted astrocytes (by Mann Whitney test; n=22 & 17 cells, N=5 & 6 mice).

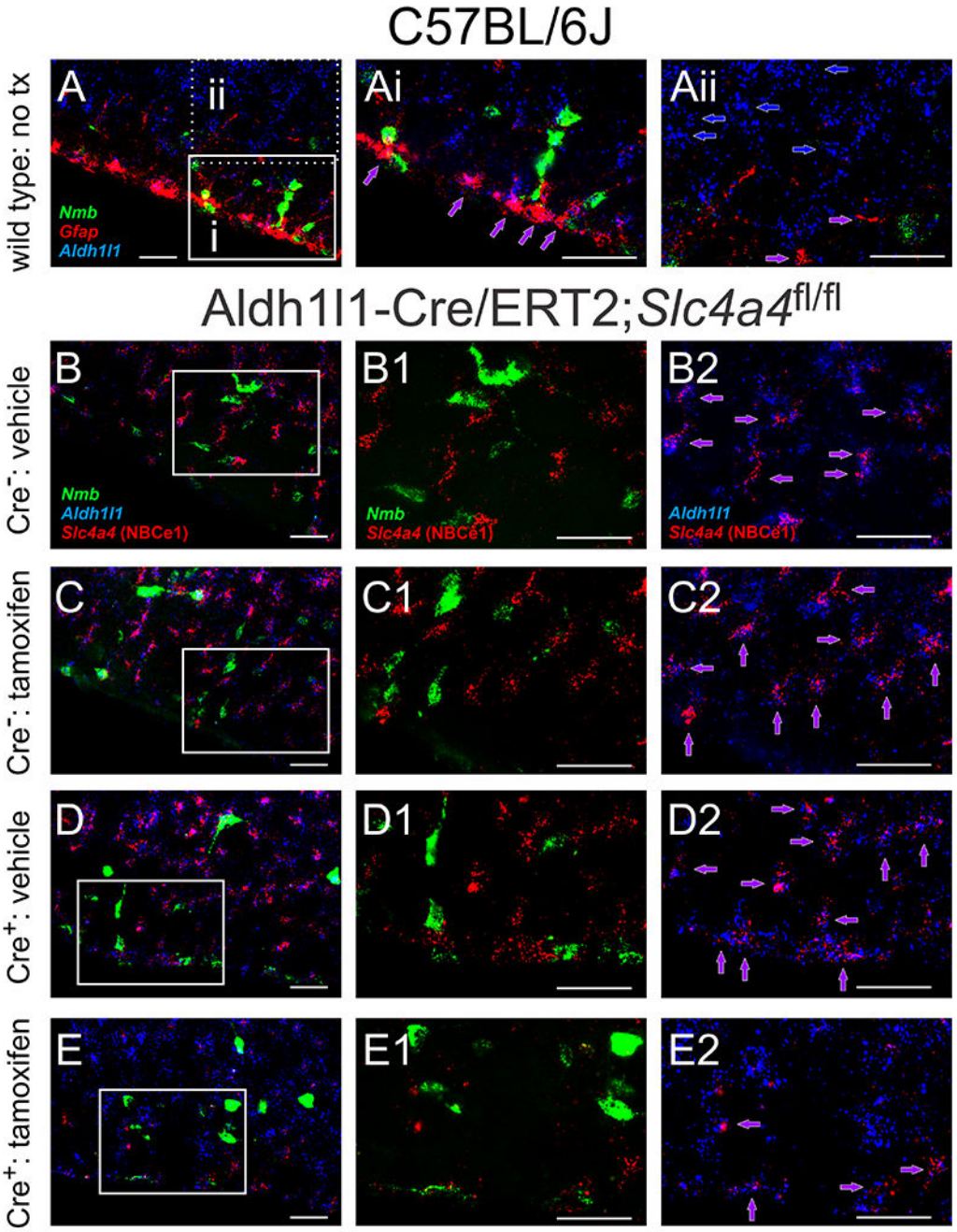

Figure 5. NBCe1 depletion in Cre-positive, tamoxifen-treated Aldh1l1-Cre/ERT2;*Slc4a4*$^{fl/fl}$ mice.
A. RNAscope for *Nmb*, *Gfap* and *Aldh1l1* in brainstem sections from control mice (C57BL/6J). Arrows indicate cells expressing: purple, *Gfap/Aldh1l1*; blue, *Aldh1l1*. Note that high *Gfap*-expression is largely confined to astrocytes on or near the ventral medullary surface. Sections at ~−6.48 mm, relative to bregma; scale bars: 50 μm. Representative of N=3 mice. **B-E.** RNAscope for *Nmb*, *Aldh1l1* and *Slc4a4* in brainstem sections from Cre-negative (**B,C**) and Cre-positive (**D,E**) Aldh1l1-Cre/ERT2;*Slc4a4*$^{fl/fl}$ mice treated either with vehicle (**B,D**) or tamoxifen (**C,E**). Arrows indicate cells expressing: purple, *Aldh1l1/Slc4a4*. Note

that prominent reduction in *Slc4a4* (NBCe1) expression selectively in Cre^{+} and tamoxifen-treated mice. Sections at ~−6.48 mm, relative to bregma; scale bars: 50 μm. Representative of N=4, 7, 5, & 5 mice.

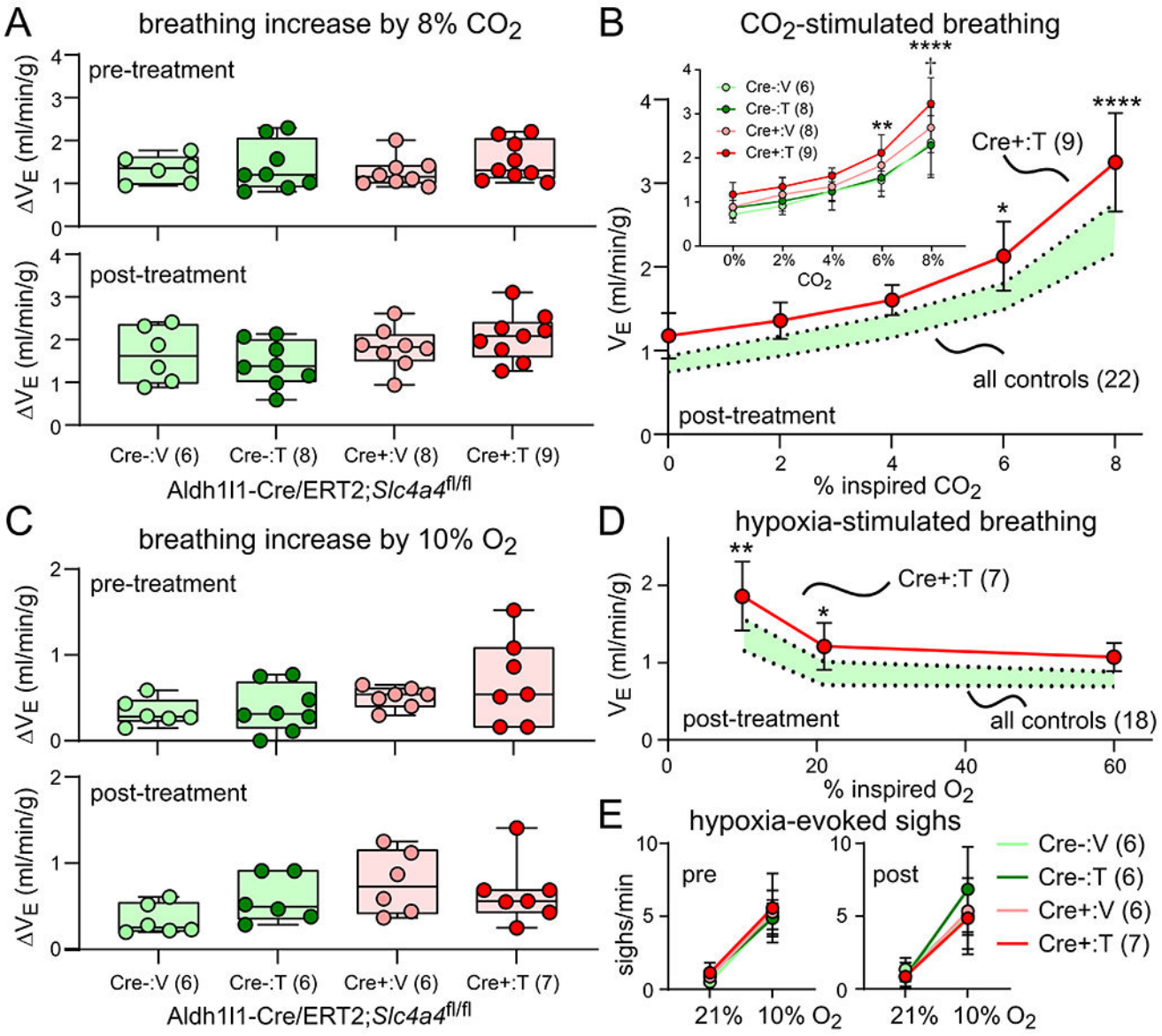

Figure 6. Effects of CO_2 and O_2 on minute ventilation and sigh frequency are unaffected by NBCe1 deletion from astrocytes in Aldh1l1-Cre/ERT2;*Slc4a4*$^{fl/fl}$ mice.

A. Increase in minute ventilation (V_E) by 8% CO_2 in the indicated groups of Aldh1l1-Cre/ERT2;*Slc4a4*$^{fl/fl}$ mice before and after treatment with vehicle or tamoxifen (ANOVA pre: $F_{3,27}$=0.5080, P=0.6801; ANOVA post: $F_{3,27}$=2.069, P=0.1279). Number of mice (N) for each group is indicated on each of the figure panels.

B. Effects of increasing inspired CO_2 (from 0% to 8%; 60% O_2, balance N_2) on V_E (mean ± SD) in each of the indicated groups of Aldh1l1-Cre/ERT2;*Slc4a4*$^{fl/fl}$ mice (*Inset*; $F_{3,135}$=16.66, P<0.0001, for genotype-treatment by 2-way ANOVA; **, P<0.005, ****, P<0.0001 for Cre^- vs. Cre^+:T; †, P=0.0121, for Cre^+:V vs. Cre^+:T) and comparing the conditional knockout mice (Cre^+:T, mean ± SD) to pooled values from all control mice

(shaded area represents the 95% confidence interval; $F_{1,145}$=41.60, P<0.0001, for genotype-treatment by 2-way ANOVA; *, P=0.0111, ****, P<0.0001 for controls vs. Cre^{+}:T).

C. Increase in V_E by hypoxia (10% O_2) in the indicated groups of Aldh1l1-Cre/ERT2;*Slc4a4*$^{fl/fl}$ mice before and treatment with vehicle or tamoxifen (ANOVA pre: $F_{3,24}$=1.905, P=0.1557; ANOVA post: $F_{3,21}$=1.767, P=0.1843).

D. Effects of varied inspired O_2 (10% O_2, 21% O_2, 60% O_2; balance N_2) on V_E comparing conditional knockout mice (Cre^{+}:T, mean ± SD) to pooled values from all control mice (area represents the 95% confidence interval; $F_{1,68}$=21.17, P<0.0001, for genotype-treatment by 2-way ANOVA; **, P=0.0025, *, P=0.491, for controls vs. Cre^{+}:T).

E. Effects of hypoxia on sigh frequency (mean ± SD) in Cre-negative and Cre-positive Aldh1l1-Cre/ERT2;*Slc4a4*$^{fl/fl}$ mice pre- and post-treatment with vehicle or tamoxifen. Hypoxia evoked sighs in all groups before and after treatment (pre: $F_{1,48}$=183.6, P<0.0001; post: $F_{1,42}$=82.37, P<0.0001, for hypoxia, by 2-way ANOVA), but there was no difference among any of the groups (pre: $F_{3,48}$=0.2274, P=0.8769; post: $F_{3,42}$=1.038, P=0.3857, for interaction by 2-way ANOVA).

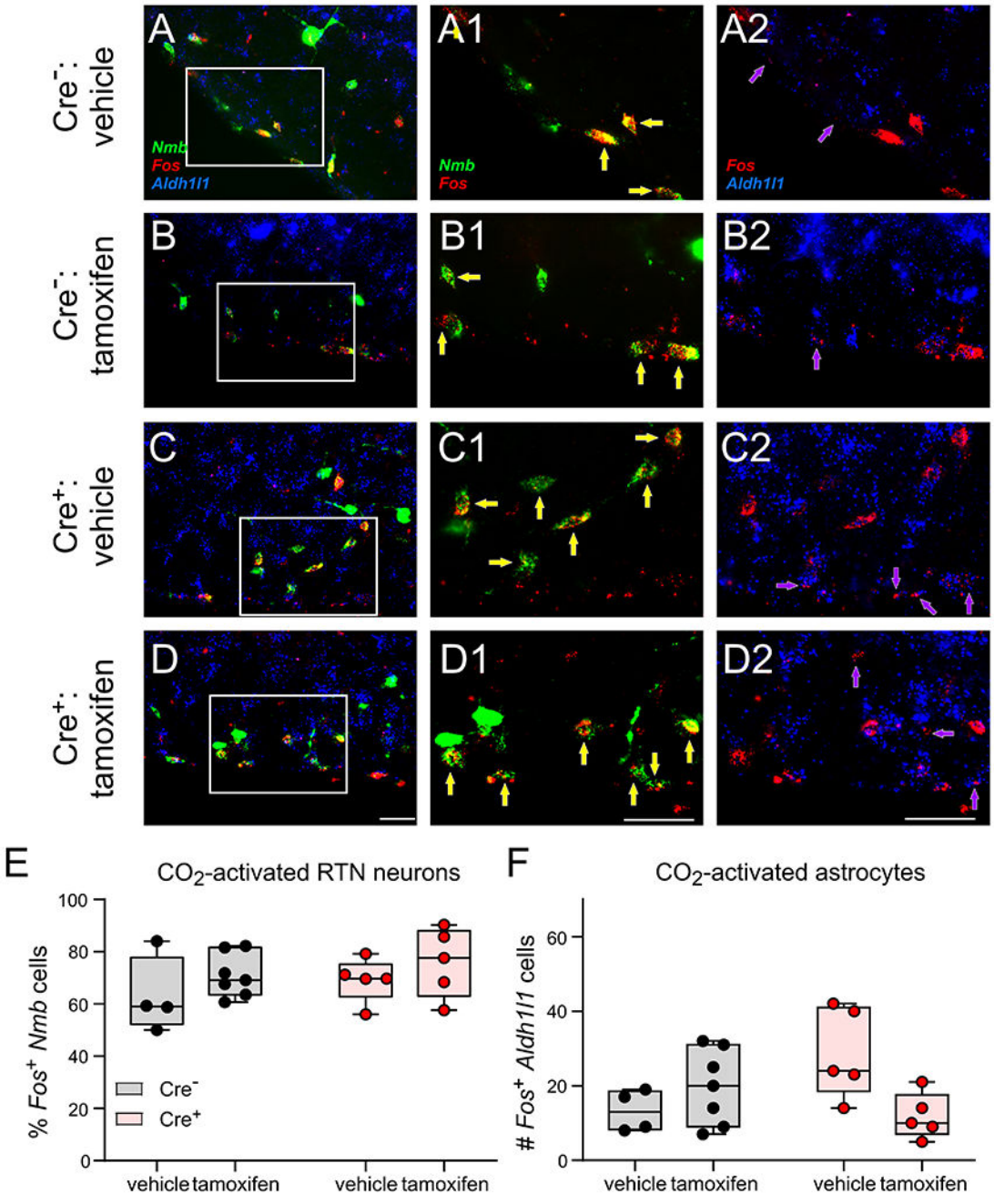

Figure 7. CO_2-stimulated Fos expression in the RTN region of Aldh1l1-Cre/ERT2;*Slc4a4*$^{fl/fl}$ mice.

A-D. RNAscope for *Nmb*, *Aldh1l1* and *Fos* (as indicated) in brainstem sections from Cre-negative (**A,B**) and Cre-positive (**C,D**) Aldh1l1-Cre/ERT2;*Slc4a4*$^{fl/fl}$ mice which were treated with vehicle (**A,C**) or tamoxifen (**B,D**) and exposed *in vivo* to 12% CO_2 (60% O_2, balance N_2). Arrows indicate cells expressing: yellow, *Nmb/Fos*; purple, *Aldh1l1/Fos*. Sections at ~−6.48 mm, relative to bregma; scale bars: 50 μm.

E,F. Quantification of percentage of *Fos*$^{+}$ RTN neurons (**E**, *Nmb*$^{+}$ cells) and number of nearby *Fos*$^{+}$ astrocytes (**F**, *Aldh1l1*$^{+}$ cells) in the RTN region of the indicated groups of Aldh1l1-Cre/ERT2;*Slc4a4*$^{fl/fl}$ mice after exposure to 12% CO_2 (60% O_2, balance N_2). 2-way ANOVA for CO_2-activated RTN neurons: interaction $F_{1,17}$=0.01331, P=0.9095; for CO_2-activated astrocytes: interaction $F_{1,17}$=8.114, P=0.0111; no differences among experimental groups by post hoc Šídák's multiple comparisons test. Sections quantified from N=4, 7, 5 & 5 mice (35.8 ± 9.9, 46.0 ± 8.4, 51.0 ± 19.0 & 34.4 ± 10.2 Nmb^{+} neurons per section).

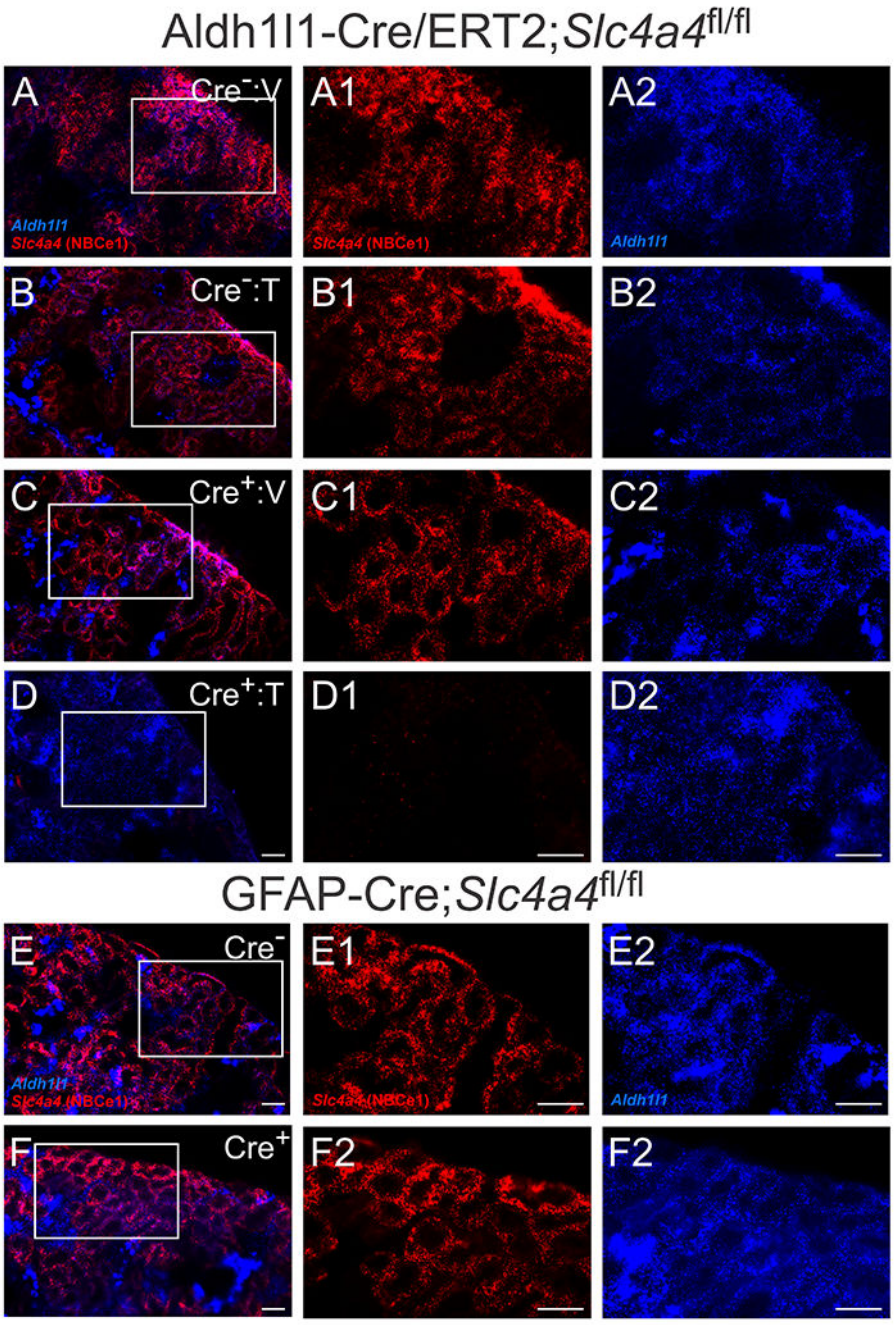

Figure 8. NBCe1 is depleted in the kidney of Cre-positive, tamoxifen-treated Aldh1l1-Cre/ERT2;*Slc4a4*$^{fl/fl}$ mice.

A-F. RNAscope for *Aldh1l1* and *Slc4a4* (NBCe1) in kidney sections from Aldh1l1-Cre/ERT2;*Slc4a4*$^{fl/fl}$ mice (**A-D**) or GFAP-Cre;*Slc4a4*$^{fl/fl}$ mice (**E,F**) that were Cre-negative (**A,B,E**) or Cre-positive (**C,D,F**) and untreated (**E,F**) or treated with either vehicle (**A,C**) or tamoxifen (**B,D**). Scale bars: 50 μm. Representative of N=3, 3, 3, & 4 Aldh1l1-Cre/ERT2;*Slc4a4*$^{fl/fl}$ mice and N=3 & 3 GFAP-Cre;*Slc4a4*$^{fl/fl}$ mice.

Table 1.

Tail arterial blood gas analysis from Aldh1l1-Cre/ERT2:*Slc4a4*$^{fl/fl}$ mice. Data are mean ± SD. Individual control groups were compared to the Cre-positive, tamoxifen-treated conditional knockouts (Cre^{+}:T) by ANOVA with post hoc Dunnett's test; pooled control data was compared to Cre^{+}:T conditional knockouts by unpaired t-tests.

	Cre^{-}:V (8)	**Cre^{-}:T (14)**	**Cre^{+}:V (10)**	**Cre^{+}:T (10)**	**all control (32)**
pH	7.40 ± 0.10 ****	7.42 ± 0.05 ****	7.39 ± 0.08 ****	7.21 ± 0.07	7.41 ± 0.07 ****
HCO_3^- (mM)	19.1 ± 3.8 ****	21.8 ± 2.7 ****	18.1 ± 4.1 ****	10.5 ± 2.1	19.9 ± 3.8 ****
PCO_2 (mmHg)	30.3 ± 4.3 *	33.0 ± 3.4 ***	29.3 ± 4.6	25.7 ± 3.3	31.1 ± 4.2 ***
PO_2 (mmHg)	88.1 ± 9.3	90.6 ± 6.7	91.3 ± 11.3	97.7 ± 7.4	90.2 ± 8.8 *
sO2 (%)	96.6 ± 1.4	97.1 ± 0.9	97.0 ± 1.1	96.1 ± 1.0	97.0 ± 1.1 *
lactate (mM)	2.9 ± 1.1	3.5 ± 1.4 *	3.9 ± 1.6 **	2.0 ± 0.9	3.5 ± 1.4 **

*'P<0.05,

**'P<0.01,

***'P<0.0005,

****'P<0.0001.

Table 2.

Tail arterial blood gas analysis from GFAP-Cre:*Slc4a4*$^{fl/fl}$ mice. Data are mean ± SD. Cre^{-} and Cre^{+} littermates were compared by unpaired t-tests.

	Cre-negative (8)	**Cre-positive (11)**
pH	7.38 ± 0.10	7.38 ± 0.05
HCO_3^- (mM)	19.7 ± 2.2	17.5 ± 3.0
PCO_2 (mmHg)	33.8 ± 6.4	29.2 ± 3.9
PO_2 (mmHg)	88.3 ± 6.6	91.0 ± 5.4
sO2 (%)	96.6 ± 1.1	97.2 ± 0.8
lactate (mM)	5.0 ± 2.2	5.8 ± 2.1